The Journal of Physiology

5-HT7 receptors expressed in the mouse parafacial region are not required for respiratory chemosensitivity

Yingtang Shi[1], Cleyton R. Sobrinho[2], Jaseph Soto-Perez[3], Brenda M. Milla[3], Daniel S. Stornetta[1], Ruth L. Stornetta[1], Ana C. Takakura[4], Daniel K. Mulkey[3], Thiago S. Moreira[2] and Douglas A. Bayliss[1]

[1]*Department of Pharmacology, University of Virginia, Charlottesville, VA, USA*
[2]*Department of Physiology and Biophysics, Institute of Biomedical Science, University of São Paulo, São Paulo, Brazil*
[3]*Department of Physiology and Neurobiology, University of Connecticut, Storrs, CT, USA*
[4]*Department of Pharmacology, Institute of Biomedical Science, University of São Paulo, São Paulo, Brazil*

Edited by: Harold Schultz & Daniel Zoccal

Linked articles: This article is highlighted in a Perspective article by Zoccal. To read this article, visit https://doi.org/10.1113/JP283142.

The peer review history is available in the Supporting information section of this article (https://doi.org/10.1113/JP282279#support-information-section).

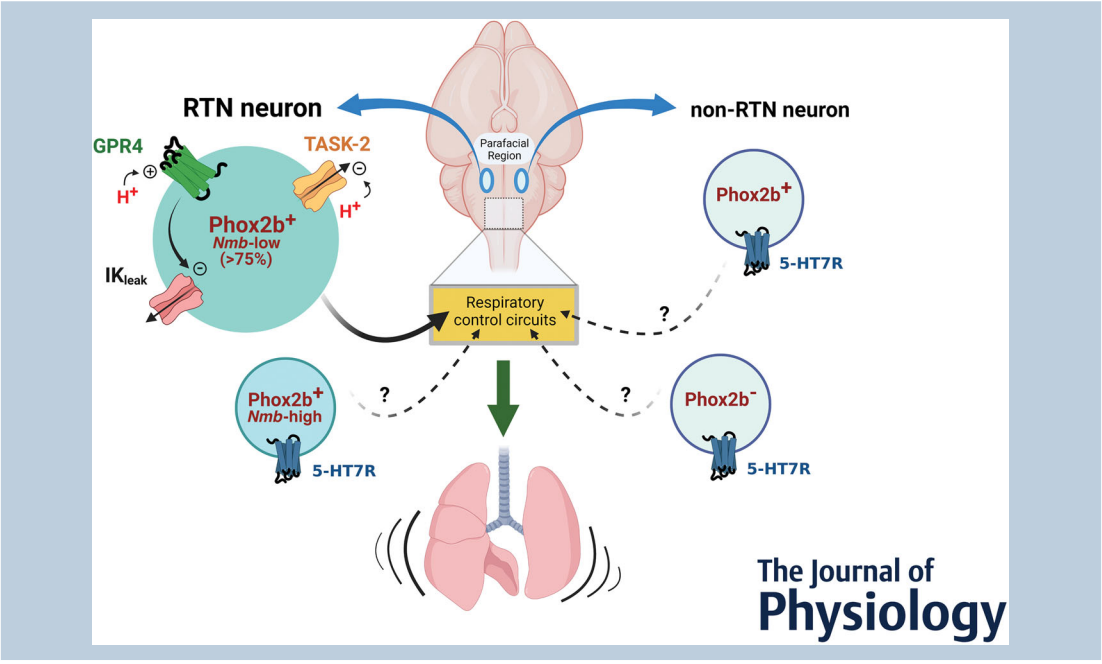

Yingtang Shi received her MD in Human Anatomy, Histology and Embryology from Shanghai Jiao Tong University School of Medicine, China. She undertook postdoctoral training in the Department of Neuroscience at the University of Virginia before moving to the Department of Pharmacology where she is an Assistant Professor of Research. She is currently investigating neuropeptides and transcription factors involved in central respiratory control during development, physiological challenge and disease conditions. **Cleyton R. Sobrinho** is currently a postdoctoral fellow at the Institute of Biomedical Science, University of São Paulo (ICB-USP). His major research interest has been focused on central mechanisms of cardiorespiratory control, including astrocyte–neuron signalling and neural networks with an emphasis on purinergic, cholinergic, histaminergic and serotonergic signalling.

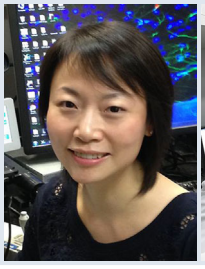

Y. Shi and C. R. Sobrinho contributed equally to this study.

DOI: 10.1113/JP282279

Abstract A brainstem homeostatic system senses CO_2/H^+ to regulate ventilation, blood gases and acid–base balance. Neurons of the retrotrapezoid nucleus (RTN) and medullary raphe are both implicated in this mechanism as respiratory chemosensors, but recent pharmacological work suggested that the CO_2/H^+ sensitivity of RTN neurons is mediated indirectly, by raphe-derived serotonin acting on 5-HT7 receptors. To investigate this further, we characterized *Htr7* transcript expression in phenotypically identified RTN neurons using multiplex single cell qRT-PCR and RNAscope. Although present in multiple neurons in the parafacial region of the ventrolateral medulla, *Htr7* expression was undetectable in most RTN neurons (Nmb^+/Phox2b$^+$) concentrated in the densely packed cell group ventrolateral to the facial nucleus. Where detected, *Htr7* expression was modest and often associated with RTN neurons that extend dorsolaterally to partially encircle the facial nucleus. These dorsolateral $Nmb^+/Htr7^+$ neurons tended to express *Nmb* at high levels and the intrinsic RTN proton detectors *Gpr4* and *Kcnk5* at low levels. In mouse brainstem slices, CO_2-stimulated firing in RTN neurons was mostly unaffected by a 5-HT7 receptor antagonist, SB269970 ($n = 11/13$). At the whole animal level, microinjection of SB269970 into the RTN of conscious mice blocked respiratory stimulation by co-injected LP-44, a 5-HT7 receptor agonist, but had no effect on CO_2-stimulated breathing in those same mice. We conclude that *Htr7* is expressed by a minor subset of RTN neurons with a molecular profile distinct from the established chemoreceptors and that 5-HT7 receptors have negligible effects on CO_2-evoked firing activity in RTN neurons or on CO_2-stimulated breathing in mice.

(Received 27 August 2021; accepted after revision 23 March 2022; first published online 6 April 2022)
Corresponding authors D. K. Mulkey, T. S. Moreira and D. A. Bayliss: Box 800735, 1300 Jefferson Park Avenue, Charlottesville, VA 22908, USA. Email: daniel.mulkey@uconn.edu; tmoreira@icb.usp.br; dab3y@virginia.edu

Abstract figure legend In the parafacial region of the mouse brainstem, the major population of Phox2b- and Neuromedin B (*Nmb*)-expressing respiratory chemosensory neurons of the retrotrapezoid nucleus (RTN) sense CO_2/H^+ via the proton detectors, G protein-coupled receptor 4 (GPR4) and TWIK-related acid-sensitive K^+ channel 2 (TASK-2). These cells express low to undetectable levels of 5-HT7 receptors, and their CO_2-stimulated firing is independent of 5-HT7R activity (upper left). 5-HT7R is localized to a minor subgroup of RTN neurons that express *Nmb* at high levels, but little if any GPR4 or TASK-2 (lower left). In addition, 5-HT7R is also expressed in some other Phox2b$^+$ and Phox2b$^-$ neurons in the parafacial region (right). However, the chemosensory role of these various 5-HT7R-expressing parafacial cells is uncertain, and blocking 5-HT7R activity in the region has no effect on CO_2-stimulated breathing in mice.

Key points

- Neurons of the retrotrapezoid nucleus (RTN) are intrinsic CO_2/H^+ chemosensors and serve as an integrative excitatory hub for control of breathing.
- Serotonin can activate RTN neurons, in part via 5-HT7 receptors, and those effects have been implicated in conferring an indirect CO_2 sensitivity.
- Multiple single cell molecular approaches revealed low levels of 5-HT7 receptor transcript expression restricted to a limited population of RTN neurons.
- Pharmacological experiments showed that 5-HT7 receptors in RTN are not required for CO_2/H^+-stimulation of RTN neuronal activity or CO_2-stimulated breathing.
- These data do not support a role for 5-HT7 receptors in respiratory chemosensitivity mediated by RTN neurons.

Introduction

An interoceptive homeostatic system for control of breathing involves sensors within the brainstem that detect CO_2 and provide a proportional drive to respiratory rhythm and pattern generating circuits to dynamically regulate ventilation and CO_2 excretion (Del Negro et al., 2018; Feldman et al., 2003; Guyenet & Bayliss, 2015; Guyenet et al., 2019). This phenomenon – central respiratory chemoreception – has been recognized for over a century and localized to the ventral brainstem

for at least 50 years (Haldane & Priestley, 1905; Mitchell et al., 1963). However, the precise cells that serve as the relevant chemosensors have remained contentious. In this respect, substantial evidence has accrued supporting involvement of multiple cell types: serotonergic neurons in the medullary raphe, glutamatergic retrotrapezoid nucleus (RTN) neurons in the parafacial medullary region and astrocytes in the rostroventrolateral medulla have been implicated as the critical sensory cells. In particular, each group is reportedly capable of directly detecting CO_2/H^+ and contributing to CO_2-regulated breathing (Brust et al., 2014; Gourine et al., 2005, 2010; Guyenet & Bayliss, 2015; Guyenet et al., 2019; Mulkey et al., 2004; Teran et al., 2014; Turovsky et al., 2016; Wang, Shi et al., 2013).

Among these cell groups, RTN neurons are particularly notable as they are indispensable for central respiratory chemoreception. For example, genetic or acute chemotoxic ablation of the putative RTN chemoreceptor neurons, or genetic deletion of two intrinsic molecular proton detectors expressed by RTN neurons (GPR4, TASK-2) essentially eliminates CO_2-stimulated breathing (Dubreuil et al., 2008, 2009; Gestreau et al., 2010; Kumar et al., 2015; Ramanantsoa et al., 2011; Souza et al., 2018; Wang, Benamer et al., 2013). This aligns with the contention that RTN neurons represent a key nodal point for both direct CO_2/H^+ chemosensation and integration/transmission of respiratory drive originating from other putative chemoreceptors (Guyenet & Bayliss, 2015; Guyenet et al., 2019; Moreira et al., 2021). Indeed, CO_2-sensitive astrocytes were hypothesized to activate RTN neurons via paracrine purinergic actions to mediate their respiratory effects (Gourine et al., 2010). Likewise, it has long been clear that serotonin (5-hydroxytryptophan, 5-HT) and other raphe-derived transmitters can activate RTN neurons (Hawkins et al., 2015; Hawryluk et al., 2012; Moreira et al., 2021; Mulkey et al., 2007; Shi et al., 2016). However, despite abundant evidence that RTN neurons are intrinsically sensitive to CO_2/H^+ (Gestreau et al., 2010; Guyenet & Bayliss, 2015; Guyenet et al., 2019; Kumar et al., 2015; Mulkey et al., 2004; Wang, Benamer et al., 2013; Wang, Shi et al., 2013), it was recently suggested instead that the chemosensitivity of RTN neurons is largely conferred indirectly, at least in part by effects of serotonin released from CO_2-sensitive raphe neurons acting specifically via 5-HT7 receptors on RTN neurons (Wu et al., 2019). In this conception, RTN neuron contributions to central respiratory chemoreception, both as sensors and integrators, derive secondarily from effects of raphe neurons and 5-HT7 receptor activation (Wu et al., 2019).

To address the possibility that 5-HT7 receptors play a critical role in RTN neuronal chemosensitivity, we assessed expression of *Htr7* transcripts in mouse RTN neurons defined by their characteristic molecular signature (Cleary et al., 2021; Shi et al., 2017; Stornetta et al., 2006). We also used receptor pharmacology to examine whether 5-HT7 receptor antagonists interfered with either RTN neuronal chemosensitivity *in vitro* or CO_2-stimulated breathing *in vivo*. We observed clear *Htr7* expression in the parafacial region, particularly in P12 mice; *Htr7* expression level decreased markedly in adult mice. Although many parafacial *Htr7*$^+$ neurons also expressed Phox2b, a non-specific marker exploited in the previous study implicating 5-HT7 in RTN chemoreception (Wu et al., 2019), *Htr7* expression was rarely detected in parafacial neurons with the molecular profile characteristic of RTN chemoreceptors (Neuromedin B (*Nmb*), *Gpr4*, *Kcnk5*) – and then at low levels. Accordingly, neither RTN neuronal CO_2/H^+ sensitivity nor CO_2-stimulated breathing was affected by SB269970, a competitive 5-HT7 receptor blocker (Hagan et al., 2000). Collectively, these data suggest minimal, if any, contribution of 5-HT7 receptor signalling to RTN neuron-mediated respiratory chemosensitivity.

Methods

Ethical approval

Experiments were performed on mice following procedures adhering to US National Institutes of Health Animal Care and Use Guidelines and approved by the Animal Care and Use Committees of the University of Virginia (Protocol no. 2454), University of Connecticut (Protocol no. A19-048), and University of São Paulo (Protocol no. 2781260620). All efforts were taken to minimize pain and suffering. The investigators understand the ethical principles under which *The Journal* operates and that the present work complies with this animal ethics checklist.

Animals

Mice were housed in HEPA-ventilated racks and steam-sterilized caging (up to five per cage), with *ad libitum* access to food and water. Animals were exposed to 12 h light/dark cycles in a vivarium maintained at 22−24°C and ∼40–50% relative humidity. To characterize *Htr7* expression, we used a Phox2b::GFP BAC transgenic mouse line (Jx99, mixed background) developed by the GENSAT project and characterized previously (Lazarenko et al., 2009). We also used a reporter mouse line obtained from crossing Phox2b::Cre BAC transgenic mice (B6(Cg)-Tg(Phox2b-cre)3Jke/J; The Jackson Laboratory, Bar Harbor, ME, USA, stock no. 016223; Rossi et al., 2011) to Ai9 or Ai14 Cre-dependent mTomato reporter mice (B6.Cg-*Gt(ROSA)26Sor*$^{tm9(CAG\text{-}tdTomato)Hze}$/J or B6.Cg-*Gt(ROSA)26Sor*$^{tm14(CAG\text{-}tdTomato)Hze}$/J; The Jackson Laboratory, stock nos 007909 or 007914); these

Table 1. RNAScope probes from advanced cell diagnostics

Transcript	ACD cat. no.	Channel	No. of pairs	Targeted region (accession number)
Nmb (Neuromedin B)	459931	1, 2	14	14–685 (NM_001291280.1)
Chat (Choline acetyltransferase)	408731	2	20	1090–1952 (NM_009891.2)
Htr7 (5-HT7 receptor)	401321	3	20	1516–2490 (NM_008315.2)
Gpr4 (GPR4)	427941	1	20	866–1900 (NM_175668.4)
Kcnk5 (TASK-2)	427951	1	20	332–1272 (NM_021542.4)

The Advanced Cell Diagnostics (ACD, Newark, CA, USA) catalogue number and detection channel for each of the transcripts detected by RNAscope. The targeted region listed covers the nucleotides in the sequence provided (see accession no.) and represents the binding region for the indicated number of ZZ paired-probes.

animals will be called Phox2b-mTom mice. Cellular electrophysiology and behavioural experiments were performed using either wild-type mice on a C57BL/6J background (The Jackson Laboratory stock no. 000664) or Phox2b-mTom mice (Ai14). A total of 105 mice of either sex were used: 13 adults (P100) and 23 juvenile (P12) mice for qRT-PCR and *in situ* hybridization experiments; 25 for single cell qPCR; 44 neonates (P7–P12) for *in vitro* electrophysiological recording; seven adults (8–15 weeks) for RTN injection and plethysmography studies).

Multiplex *in situ* hybridization

Anaesthetized mice (ketamine, 75 mg kg^{-1}; xylazine, 5 mg kg^{-1}; I.P.) were examined for absence of response to a firm toe pinch and perfused transcardially with 4% paraformaldehyde–0.1 M phosphate buffer (PB). Brains were removed, immersed in the same fixative for 16−18 h at 4°C, cut in the transverse plane (30 μm) and placed in cryoprotectant (30% ethylene glycol, 20% glycerol, 50 mM PB, pH 7.4) at −20°C until further processing. Tissue preparation and staining procedure utilized the RNAscope Multiplex Fluorescent Assay (Advanced Cell Diagnostics (ACD), Newark, CA, USA; RRID:SCR_012481), according to the manufacturer's instructions, as previously described (Shi et al., 2017, 2021). Catalogue probes were used for *Nmb*, *Chat*, *Htr7*, *Gpr4* and *Kcnk5* (Table 1).

In some experiments, multiplex *in situ* hybridization was combined with immunohistochemical detection of Phox2b and/or mTomato (Shi et al., 2016, 2021). For this, sections were first processed by the RNAscope protocol (as above) and then rinsed for 10 min in blocking buffer (10% horse serum, 0.1% Triton X-100 in 100 mM Tris buffer), incubated in blocking buffer containing primary antibody to Phox2b or mTomato (4°C, overnight; 1:100, goat α-Phox2b, R&D Systems, Minneapolis, MN, USA, AB_10889846; 1:1000 rabbit α-dsRed, Takara Biosciences, San Jose, CA, USA, AB_10013483). Sections were rinsed 2 × 2 min in Tris buffer, incubated for 30 min in Tris buffer with secondary antibody (1:400, donkey α-goat-Alexa 488, AB_2340437; or 1:400, donkey α-rabbit-Cy3, AB_2307443; both Jackson ImmunoResearch Laboratories, West Grove, PA, USA), rinsed and allowed to air dry. Slides were covered with Prolong Gold with DAPI Anti-fade mounting medium (Thermo Fisher Scientific, Waltham, MA, USA).

Cell counts, mapping and analysis

Serial (1:3 series) 30 μm transverse sections through the rostrocaudal brainstem were examined for each experiment under bright-field and epifluorescence using a Zeiss AxioImager Z.1 or a Zeiss AxioImager M2 microscope (Carl Zeiss Microscopy, White Plains, NY, USA) equipped with Neurolucida software (MBF Bioscience, Williston, VT, USA; RRID:SCR_001775) following methods previously described (Shi et al., 2017; Stornetta et al., 2004). Sections were aligned as closely as possible to brain levels with reference to bregma using the atlas of (Franklin & Paxinos, 2013). Labelled cells were counted and mapped bilaterally. Most mapping was limited to the ventral half of the brainstem which contains the distinctive and isolated parafacial cluster of Nmb^+ neurons. Photographs were taken with a Hamamatsu Photonics (Hamamatsu, Japan) C11440 Orca-Flash 4.0LT digital camera (resolution 2048 × 2048 pixels) and the resulting TIFF files were imported into CorelDRAW X7 (Corel, Ottawa, Canada; RRID:SCR_014235) for labelling and final presentation. Labelled cells were counted and aligned for averaging according to defined anatomical landmarks (Franklin & Paxinos, 2013). No stereological correction factor was applied.

Single-cell molecular biology of RTN neurons

For single neuron collection from Jx99 mice, transverse brainstem slices were prepared as previously described (Shi et al., 2016, 2021). For neonates, mice were chilled by hypothermia (<P5) or anaesthetized with ketamine and

Table 2. Primer sequences for quantitative RT-PCR

Transcript	Primers (5′ to 3′)	Amplicon	Accession no.
Gapdh	GCAAATTCAACGGCACAGTCAAGG		NM_008084.3
	TCTCGTGGTTCACACCCATCACAA	255	
Nmb	GCTCTTCGCATTGTTCGCT		NM_026523.4
	GGGGGTTCCAGGCTCTTCTT	148	
Htr7 (5-HT7)	CTATGGCAGAGTCGAGAAA		NM_008315.3
	CAATCAGGTAGTTGGAGGG	137	
Gpr4	CTTCATCTCCACTCCTCAGTCTC		NM_175668.4
	GGAAGGGATGCTAGGAAACAGGA	131	
Kcnk5(TASK-2)	CATCACCACCATCGGTTATGGCAA		NM_021542.4
	ACACGTGATCTGAGCCTTCCTCA	201	

The 5′ and 3′ primers used for quantitative RT-PCR for the indicated transcripts (with accession no.) from brainstem and single RTN neurons.

xylazine (375 mg kg^{-1} and 25 mg kg^{-1}, intramuscularly, P6–P12); after establishing no response to firm toe pinch, the mice were rapidly decapitated, and brainstems were immediately removed and sliced (300 μm) using a vibrating microslicer (DTK Zero 1; Ted Pella, Inc., Redding, CA, USA) in ice-cold, sucrose-substituted Ringer solution containing the following (in mM): 260 sucrose, 3 KCl, 5 $MgCl_2$, 1 $CaCl_2$, 1.25 NaH_2PO_4, 26 $NaHCO_3$, 10 glucose, and 1 kynurenic acid. Individual green fluorescent protein (GFP)-labelled RTN neurons were harvested under direct vision from mouse brainstem slices ($n = 176$, $N = 25$) in a Hepes-based solution (mM): 140 NaCl, 3 KCl, 2 $MgCl_2$, 2 $CaCl_2$, 10 Hepes, 10 glucose, pH 7.4 at room temperature) in the recording chamber of a fluorescence microscope (Zeiss Axioimager FS, Carl Zeiss Microscopy). Neurons were targeted based on a healthy appearance (e.g. soma size and turbidity, membrane transparency, dendritic process visibility) and fluorescence intensity. A pipette loaded with a sterile Hepes-based buffer (tip diameter: ~10 μm) was advanced toward the cell, with application of gentle positive pressure to clear away nearby cellular debris and extracellular matrix (delivered by mouth, via a side port on the pipette holder with an intervening 0.22 μm sterile filter in the line). Subsequently, gentle suction was used to collect the cell, while minimizing aspiration of non-somatic cellular components. Once the cell was picked, ~1 μl of internal solution containing the cytoplasmic contents were expelled into a sterile tube containing reverse transcriptase reagents. Neurons were analysed simultaneously for expression of multiple transcripts (*Gpr4*, *Kcnk5*, *Htr7*) by multiplex quantitative sc-PCR (sc-qPCR) (Shi et al., 2016, 2021). We used primer sets for sc-qPCR that yielded short amplicons (Table 2); the cycle threshold (C_t) levels of test transcripts were re-scaled by their average, transformed into relative quantities using the amplification efficiency, normalized to *Gapdh* (an internal reference gene; $\Delta C_t = C_{t(test)} - C_{t(Gapdh)}$), and expressed as $2^{-\Delta C_t}$ (Pfaffl, 2001).

A similar single cell harvesting approach was employed to obtain cells for single cell RNA-Seq experiments performed previously. The reader is referred to Shi et al. (2017) and Stornetta et al. (2004) for detailed methods on how the transcriptomic data were obtained and analysed.

Quantitative PCR of mouse brainstem

We used standard qRT-PCR to determine age-dependent changes in 5-HT7 receptor expression in mouse brainstem. From anaesthetized mice (as above), we rapidly isolated the entire brainstem (from −5.4 mm to −7.0 mm, relative to bregma), extracted RNA (Qiagen, Germantown, MD, USA, RNA isolation Kit: 74104), and synthesized cDNA (Bio-Rad Laboratories, Hercules, CA, USA, iScriptTM cDNA Synthesis Kit: 1708891). In a 25 μl reaction containing *Gapdh* and *Htr7* primers (Table 2), 10 ng μl^{-1} cDNA was used for of quantitative PCR (iCycler iQ; Bio-Rad) thus: denaturation (95°C, 3 min); amplification and quantification (30 cycles: 95°C, 20 s; 60°C, 20 s; 72°C, 20 s); with melt curve analysis (ramp from 55°C to 95°C, 2 s increments). The *Htr7* C_t values were normalized to those of *Gapdh* and expressed as $2^{-\Delta C_t}$ (Pfaffl, 2001).

Electrophysiology in brainstem slices

Slices were prepared from the brainstem of neonatal P7-P12) wild-type mice ($N = 37$) and Phox2b-mTom mice (Ai14 strain; $N = 7$). Pups were anaesthetized with ketamine and xylazine (375 mg kg^{-1} and 25 mg kg^{-1}, I.M.). After verifying the lack of response to a firm toe pinch, pups were rapidly decapitated and medullary slices (250 μm) were cut in ice-cold sucrose-substituted

solution, containing (mM): 260 sucrose, 3 KCl, 5 $MgCl_2$, 1 $CaCl_2$, 1.25 NaH_2PO_4, 26 $NaHCO_3$, 10 D-glucose, and 1 kynurenic acid. Slices were incubated for 30 min at 37°C and subsequently at room temperature in normal Ringer solution containing (mM): 130 NaCl, 3 KCl, 2 $MgCl_2$, 2 $CaCl_2$, 1.25 NaH_2PO_4, 26 $NaHCO_3$, and 10 D-glucose. Cutting, incubation and recording solutions were bubbled with 95% O_2–5% CO_2.

Individual slices containing the RTN were transferred to a recording chamber mounted on a fixed-stage microscope (Olympus, Tokyo, Japan, BX5.1WI) and perfused continuously (∼2 ml min^{-1}) with normal Ringer solution. Recordings (1 cell/mouse) were made at room temperature or 37°C, as indicated, with an Axopatch 200B patch-clamp amplifier, digitized with a Digidata 1322A A/D converter and recorded using pCLAMP 10.0 software (Molecular Devices, San Jose, CA, USA, RRID: SCR_011323). Cellular excitability was measured in the cell-attached (seal resistance >1 GΩ) current clamp mode using a pipette solution containing (in mM): 120 KCH_3SO_3, 4 NaCl, 1 $MgCl_2$, 0.5 $CaCl_2$, 10 Hepes, 10 EGTA, 3 Mg-ATP and 0.3 GTP-Tris, 0.2% Lucifer Yellow (pH 7.30). For testing effects of CO_2/H^+, the gas mixture was switched to one containing 10% CO_2 (balance O_2) for at least 5 min or when a plateau of firing activity was achieved for at least 2 min. Serotonin (5-HT, 5−10 μm; Millipore Sigma, Burlington, MA, USA) and the 5-HT7 receptor agonist LP-44 (2 μM; Tocris Bioscience, Minneapolis, MN, USA) or antagonist SB269970 (10 μM; Tocris) were delivered via the bath. Where indicated, slices were incubated in a cocktail of synaptic blockers: 6-cyano-7-nitro-quinoxaline-2,3-dione (CNQX) (10 μM; Tocris) to block AMPA/kainate receptors, strychnine (2 μM; Sigma) to block glycine receptors, and gabazine (10 μM; Sigma) to block $GABA_A$ receptors. Firing rate histograms were generated by integrating action potential discharge in 10–15 s bins using Spike2 (v.5) software (Cambridge Electronic Design, Cambridge, UK).

To confirm that recorded cells were Phox2b-immunoreactive, slices containing Lucifer Yellow-filled cells were placed in 4% paraformaldehyde for at least 24 h at 4°C, washed in phosphate-buffered saline (PBS, 2 × 5 min), permeabilized in PBS–0.2% Triton X-100 (1× PBST, 2 × 5 min), and blocked in PBST–2% normal donkey serum (2 h). Slices were incubated overnight in fresh blocking solution containing goat anti-Phox2b antibody (1:150; R&D systems, AB_1089846) and rabbit anti-Lucifer Yellow antibody (1:450; Thermo Fisher Scientific, AB_2536190). Slices were then washed (PBST, 5 × 10 min) and incubated for 2 h in blocking solution containing donkey anti-goat Alexa 647 (AB_2340436) and donkey anti-rabbit Alexa 488 (AB_2313584, both at 1:500, from Jackson ImmunoResearch); immunolabelling was not needed for imaging mTomato fluorescence in slices from Phox2b-mTom mice. Slices were washed in PBST (5 × 10 min) and PBS (5 × 10 min), mounted on fresh, pre-cleaned glass slides using Prolong Diamond with DAPI (Thermo Fisher Scientific), and imaged with a Leica SP8 confocal microscope (Leica, Wetzlar, Germany).

RTN microinjection and breathing measurements

Adult mice ($N = 7$; 8–15 weeks old) were anaesthetized with intraperitoneal injection of ketamine (100 mg kg^{-1}) combined with xylazine (7 mg kg^{-1}) and placed in a stereotaxic frame (model 900; David Kopf Instruments, Los Angeles, CA, USA). The level of anaesthesia was monitored throughout the procedures by testing for absence of withdrawal response due to firm paw pinch. Stainless steel cannulas were placed bilaterally into the RTN using the coordinates 1.2 mm caudal to lambda, 1.4 mm lateral to the midline, and 5.0 mm below dura mater. The cannulas were fixed to the cranium using dental acrylic resin and jewellers' screws. Mice received a prophylactic dose of penicillin (30,000 IU) given intramuscularly. After the surgery, the mice were given a subcutaneous injection of the analgesic Ketoflex (1%, 0.2 ml/mouse) and maintained in individual boxes with free access of tap water and food pellets.

A week after the stereotaxic surgery, when the mice had recovered, whole-body plethysmography was used to measure respiratory activity. Adult mice were placed individually into a Plexiglas recording chamber (700 ml) that was flushed continuously with a mixture of 79% nitrogen and 21% oxygen (unless otherwise required by the protocol) at a rate of 0.5 l min^{-1}. A volume calibration was performed during each experiment by injecting a known air volume (1 ml) inside the chamber. All experiments were performed at room temperature (24–26°C). Tidal volume (V_T, measured in μl, normalized to body weight and corrected to account for chamber and animal temperature, humidity, and atmospheric pressure) and respiratory frequency (f_R, breaths min^{-1}) were recorded on a breath-to-breath basis and analysed during the last 2 min of each experimental condition when breathing was stabilized; the product of tidal volume and frequency is minute ventilation ($\dot{V}_E$, μl min^{-1} g^{-1}), which was analysed over sequential 20 s epochs (∼50 breaths). Measurements of breathing activity were performed using a whole-body plethysmography closed system as described previously (Drorbaugh & Fenn, 1955). Concentrations of O_2 and CO_2 in the chamber were monitored on-line using a fast-response O_2/CO_2 monitor (ADInstruments). The pressure signal was amplified, filtered, recorded and analysed off-line using Powerlab software (Powerlab 16/30, ML880/P, ADInstruments, Colorado Springs, CO, USA).

Breathing parameters (f_R, V_T and $\dot{V}_E$) were continuously recorded, starting 30–45 min after the mice were placed

in the recording chambers. Control (baseline) values were recorded for 2 min and were analysed immediately before the first treatment (saline or SB269970 into the RTN). These values were used as a reference to calculate the changes produced by the treatments. LP-44 (2 mM, 50 nl; 100 pmol) or saline (50 nl) was injected unilaterally into the RTN ∼10 min after the bilateral injection of SB269970 (1 mM, 50 nl; 50 pmol) or saline in the same place. For the CO_2 challenge, the protocol included three sequential incrementing CO_2 challenges (7 min exposures to 2%, 4%, 6%, 8% and 10% CO_2, balance O_2; each separated by 5 min of 100% O_2, and presented in random order). The CO_2 exposures were performed immediately prior to and then ∼10 min after bilateral injection of SB269970 or saline. Hypercapnic exposure was performed in hyperoxia to minimize contributions of peripheral chemoreceptors to the hypercapnic ventilatory reflex (Basting et al., 2015) and to attribute ventilatory effects to central chemoreceptors. For analysis of the hypercapnic ventilatory response, we sampled 10 consecutive epochs (200 s, representing ∼400–500 breaths at rest) that showed the least inter-breath irregularity during the steady-state plateau period after each CO_2 exposure, as determined by Poincaré analysis.

Histology and analysis

Following *in vivo* experiments, mice were deeply anaesthetized with ketamine/xylazine (200/14 mg kg^{-1}) and injected with heparin (50 units, transcardially) and were perfused via the ascending aorta and pulmonary artery with 50 ml of PBS (pH 7.4), followed by 100 ml of 4% paraformaldehyde (Electron Microscopy Sciences, Hatfield, PA, USA) in 0.1 M PB (pH 7.4). The brain was then removed and stored in fixative for 24–48 h at 4°C. A series of coronal sections (30 μm) were cut on a microtome (SM2010R; Leica Biosystems) and stored in cryoprotectant solution at −20°C (20% glycerol, 30% ethylene glycol in 50 mM PB) for later histological processing. All histochemical procedures were performed using free-floating sections, in accordance with previously described protocols (Shi et al., 2017, 2021). The sections were mounted onto slides, dried, covered with DPX (Millipore Sigma, Milwaukee, WI, USA), and coverslips were affixed with nail polish. Injections sites in the RTN were confirmed by inspection using an Axioskop A1 microscope (Carl Zeiss Microscopy). Consecutive sections from different brains were aligned with respect to a reference section, which was the most caudal section containing an identifiable cluster of facial motor neurons (assigned a value of −6.48 mm, caudal to bregma; Franklin & Paxinos, 2013); levels rostral or caudal to this reference section were determined by adding or subtracting the number of intervening sections (40 μm intervals). Photographs were taken with a Hamamatsu C11440 Orca-Flash 4.0LT digital camera (resolution: 2048 × 2048 pixels). A technical illustration software package (Canvas, v.9.0; ACD Systems, Victoria BC, Canada) was used for line drawings, assembly of figures and labelling according to (Franklin & Paxinos, 2013).

Statistics

Results are given as mean ± SD, and presented in violin or box and whiskers format (box bisected by median and bounded by 25%ile and 75%ile, with whiskers indicating the range). Statistical analyses were performed using GraphPad Prism (v. 9) (GraphPad Software, Inc., La Jolla, CA, USA); the details of specific tests and exact *P*-values are provided in the text, figures or figure legends.

Results

To examine the proposed role of 5-HT7 receptors in RTN neurons (Wu et al., 2019), we first evaluated *Htr7* expression in phenotypically identified RTN neurons. We then tested effects of 5-HT7 blockers on CO_2/H^+ chemosensitivity of RTN neurons *in vitro*, and on CO_2-stimulated breathing mediated by the RTN *in vivo*.

Single cell mRNA quantification reveals limited *Htr7* expression in RTN neurons

We analysed previously published single cell transcriptomic data from GFP-labelled neurons manually selected from brainstem slices of Phox2b::GFP mice (Fig. 1*A*; GEO: GSE163155) (Guyenet et al., 2019; Shi et al., 2017). In *Nmb*-expressing RTN neurons, *Htr7* expression was detected at low levels and in a subpopulation of cells (∼46%, of $n = 75$: 6.1 ± 12.7 transcripts per million, TPM). GPR4 and TASK-2 (encoded by *Kcnk5*) are the putative proton detectors that mediate intrinsic CO_2/H^+ sensitivity of RTN neurons (Gestreau et al., 2010; Kumar et al., 2015; Wang, Benamer et al., 2013). Nearly all cells expressed transcripts for *Gpr4* (∼89%; 146.8 ± 117.2 TPM), which is the most highly expressed G protein-coupled receptor in RTN neurons (Guyenet et al., 2019; Shi et al., 2017); intermediate levels of *Kcnk5* transcripts were also found in a large percentage of cells (∼83%; 17.3 ± 18.3 TPM).

To re-evaluate expression of these transcripts in RTN neurons, we again harvested single GFP-labelled neurons from brainstem slices prepared from Phox2b::GFP mice ($N = 25$) and performed multiplexed sc-qPCR for *Htr7* along with *Gpr4* and *Kcnk5* (Fig. 1*B*) (Shi et al., 2016, 2017). We verified expression of *Nmb* in the sampled GFP-positive cells ($n = 176$) to ensure that they matched the molecular profile expected of RTN neurons

(Shi et al., 2017). As expected from the transcriptomic data, we found high levels of *Gpr4* mRNA in virtually all *Nmb*$^+$ RTN neurons (∼98%, n = 173/176; $2^{-\Delta C_t}$: 0.197 ± 0.434) with intermediate levels of expression for *Kcnk5* (∼43%, n = 75/176; $2^{-\Delta C_t}$: 0.020 ± 0.018). By comparison to *Gpr4* and *Kcnk5*, and consistent with our earlier transcriptomic analysis (Guyenet et al., 2019; Shi et al., 2017), *Htr7* was expressed in fewer cells and at lower levels (∼20%, n = 36/176; $2^{-\Delta C_t}$: 0.011 ± 0.011). Note that the sensitivity of our sc-qPCR assay appears to be lower than that for scRNA-Seq, as evidenced by the reduced detection of the less abundant transcripts. Nonetheless, across both assays, the results consistently show relatively modest *Htr7* expression in *Nmb*-positive RTN neurons.

Htr7 is expressed in many Phox2b$^+$ cells and a select group of RTN neurons

We performed RNAscope multiplex *in situ* hybridization to assess *Htr7* expression across the rostrocaudal extent of the RTN and to circumvent any sampling bias associated with the single cell harvesting procedure. We assessed expression in sections from young mice (P12), around the ages used for *in vitro* electrophysiology, and from older mice (P90–P120) such as those used for *in vivo* drug injection and plethysmography (see below). As shown in low power photomicrographs, we first noted that *Htr7* expression was prominent in many regions of P12 mouse brainstem, with a marked decrease in *Htr7* expression in older mice (Fig. 1*C*). This generalized developmental decrease in *Htr7* expression was verified by qRT-PCR from the brainstem of young and adult mice (Fig. 1*D*; slice from −5.4 mm to −7.0 mm relative to bregma, referenced to adult).

We next focused on characterizing *Htr7* expression more precisely within different cell populations of the parafacial region. In this region, multiple distinct neuronal cell groups express Phox2b (Stornetta et al., 2006), the transcription factor that was used for Cre-dependent reporter gene expression in previous tests of 5-HT7 contributions to RTN neuronal chemosensitivity (Wu et al., 2019). Aside from the Phox2b-expressing RTN

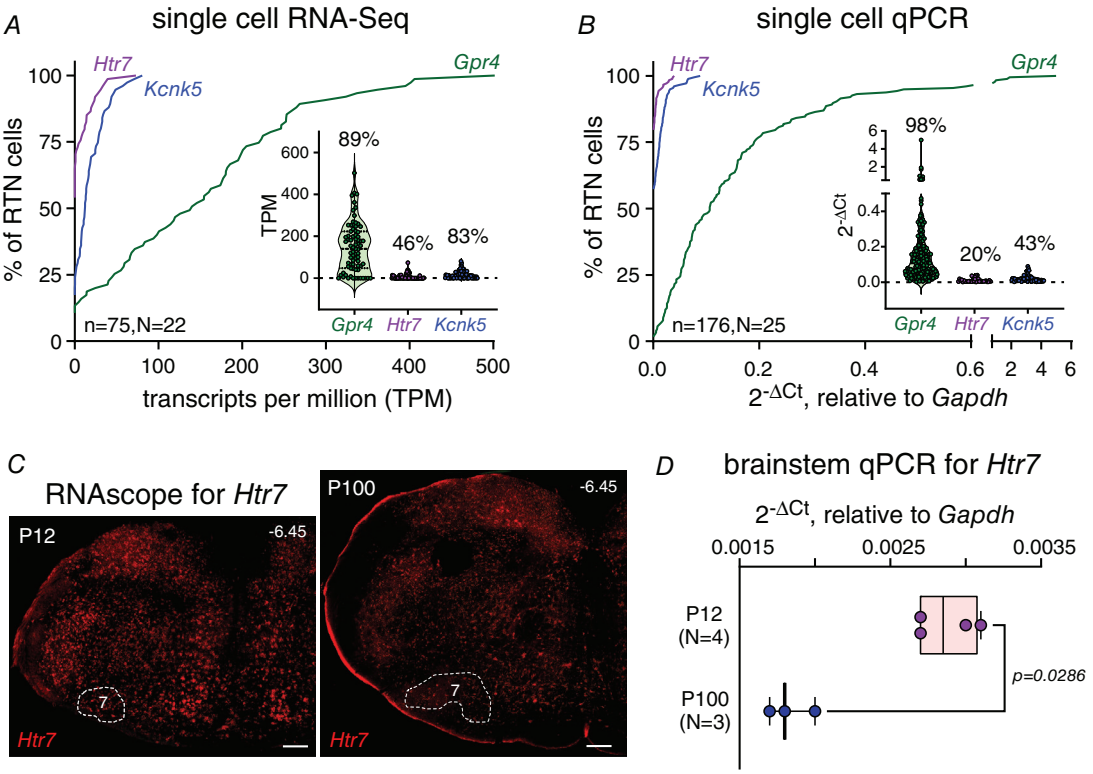

Figure 1. *Htr7* expression in RTN neurons and mouse brainstem
A and *B*, cumulative probability distributions for the indicated transcripts (*Htr7*, *Kcnk5*, *Gpr4*) in GFP-positive, *Nmb*-expressing neurons harvested from Phox2b::GFP mice for single cell RNA-Seq (*A*: n = 75, N = 22; data from Shi et al. (2017); GEO: GSE163155) and single cell multiplex qRT-PCR (*B*: n = 176, N = 25). Insets show transcript levels for all individual *Nmb*-expressing RTN neurons, with percentage of expressing neurons indicated. *C*, RNAscope *in situ* hybridization for *Htr7* in the brainstem of young (P12) and adult (P100) mice at comparable rostrocaudal levels (∼6.45 mm caudal to bregma). Scale bar: 500 μm. *D*, expression levels of *Htr7* in brainstem of young (P12, N = 4) and adult (P100, N = 3) mice by qRT-PCR; P = 0.0286, by Mann–Whitney test. [Colour figure can be viewed at wileyonlinelibrary.com]

neurons, which also uniquely express *Nmb*, the other prominent Phox2b-expressing cell groups in this region are facial motoneurons and C1 adrenergic neurons (Stornetta et al., 2006).

We used Phox2b immunostaining together with RNAscope detection of *Nmb* and *Htr7* expression to characterize *Htr7* expression in Phox2b-containing neurons generally, and in RTN neurons co-expressing Phox2b and *Nmb* specifically (Fig. 2). In the parafacial region, *Htr7* expression was observed in both Phox2b-negative (red arrows) and Phox2b-positive neurons, with distribution dependent on rostrocaudal location and developmental stage (Figs 2*A* and 3). At caudal levels in the P12 mice, strong *Htr7* labelling often coincided with Phox2b$^+$ neurons that were *Nmb*-negative and dorsomedially displaced from the main cluster of *Nmb*$^+$ cells that comprise the RTN (Fig. 2*A*–*C*: magenta circles in maps, purple arrows in photomicrographs); these are likely the Phox2b$^+$/*Nmb*$^-$ C1 neurons that are prevalent at this brainstem level (Shi et al., 2017; Stornetta et al., 2006).

Among the Phox2b$^+$/*Nmb*$^+$ RTN neurons, *Htr7* transcript expression was generally undetectable (Fig. 2*C*–*F*: blue arrows) except that it appeared most often in the larger RTN neurons with the highest levels of *Nmb* expression (Fig. 2*A*: orange triangles; Fig. 2*C*–*F*: white arrows), a group we previously deemed *Nmb*-high cells (Shi et al., 2017). At more rostral levels, particularly high levels of *Htr7* expression were evident in Phox2b$^+$ cells located in the facial motor nucleus (Fig. 2*F*: purple arrows); these cells were confirmed as motoneurons based on their co-expression of *Chat* (Fig. 4). For RTN neurons at this rostral level, *Htr7* expression was again largely confined to the *Nmb*-high cells, which often wrapped around the dorsolateral aspects of the facial motor nucleus (Fig. 4*A* and *B*). Cell counts from these sections were generally consistent with the data from single cell transcriptomic and qRT-PCR analyses in revealing that *Htr7* expression was limited to a minor population of *Nmb*-positive RTN neurons (24.4 ± 4.8%, $N = 7$). These expression patterns were similar in sections from adult mice ($N = 5$), albeit with substantially lower levels of *Htr7* expression (*Htr7* was found in 8.5 ± 2.4% of *Nmb*$^+$ neurons in adult; Figs 3 and 4*C* and *D*).

Phox2b-Cre-dependent reporter expression is observed together with *Htr7* in many *Nmb*-negative parafacial neurons

A strategy based on Phox2b-Cre-dependent reporter gene expression was used in recent experiments reporting 5-HT7 contributions to neuronal chemosensitivity in the parafacial region (Wu et al., 2019). We examined the fidelity of this reporter-based, lineage tracing approach for identification of cells that: (1) retain Phox2b expression; (2) are bona fide RTN neurons (i.e. *Nmb*$^+$ cells); and/or (3) express *Htr7* transcripts. In brainstem sections from Phox2b-mTom mice (P12), there was substantial overlap of Phox2b$^+$ and mTomato$^+$ cells in the parafacial region, and many of those cells containing both those markers also expressed *Nmb* (Fig. 5*A*). Of note, however, there was also a sizeable group of Phox2b$^+$ and mTomato$^+$ neurons that were *Nmb*-negative (i.e. they were not RTN neurons). Most of these non-RTN Phox2b$^+$/mTomato$^+$ neurons were within the confines of the facial motor nucleus, especially evident in images at more rostral levels, but they were also often found intermingled with the *Nmb*$^+$ cells or, more often, located just dorsomedially to those RTN neurons. When examined for 5-HT7 receptor transcripts (Fig. 5*B*), we found numerous *Nmb*-negative and mTomato$^+$ neurons that express *Htr7*; this was not limited only to cells in the facial motor nucleus, of which there were many, but also included the mTomato$^+$ neurons located in proximity to the *Nmb*$^+$ neurons of the RTN. Among the actual RTN neurons, *Htr7* expression was most prominently observed in the larger cells with the highest levels of *Nmb*. At intermediate rostrocaudal levels (e.g. bregma, −6.2 mm, Fig. 5*B*) where the RTN is compressed onto the ventral medullary surface by the facial nucleus, these cells cluster together with nearby *Htr7*-negative RTN neurons. So, although Cre-dependent reporter expression provides a reasonably effective identification of Phox2b- and *Nmb*-expressing RTN neurons in the parafacial region, that lineage labelling approach is imperfect and also marks many local cells that are not RTN neurons, including some that express *Htr7*.

RTN neurons that express *Htr7* have low to undetectable levels of *Gpr4* and *Kcnk5* expression

In our previous transcriptomic and histochemical analysis, we found that the dorsally located *Nmb*-high RTN neurons, unlike the majority of *Nmb*-expressing RTN neurons, expressed low to undetectable levels of the RTN proton detectors, *Gpr4* and *Kcnk5* (Shi et al., 2017). Moreover, these *Nmb*-high cells were unique among RTN neurons in that they were not demonstrably chemosensitive *in vivo* (i.e. they did not express *Fos* after exposure to CO_2) (Shi et al., 2017). In light of this, and given the association of *Htr7* expression with the *Nmb*-high group of cells, we examined *Htr7* co-expression patterns with *Gpr4* and *Kcnk5* (Fig. 6).

In the P12 mouse brainstem, *Gpr4* and *Kcnk5* transcripts were only rarely detected in *Htr7*-expressing *Nmb*-high RTN neurons, and then at lower levels than observed in RTN neurons with moderate *Nmb* expression. This pattern was more evident for *Gpr4* (Fig. 6*A*–*C*)

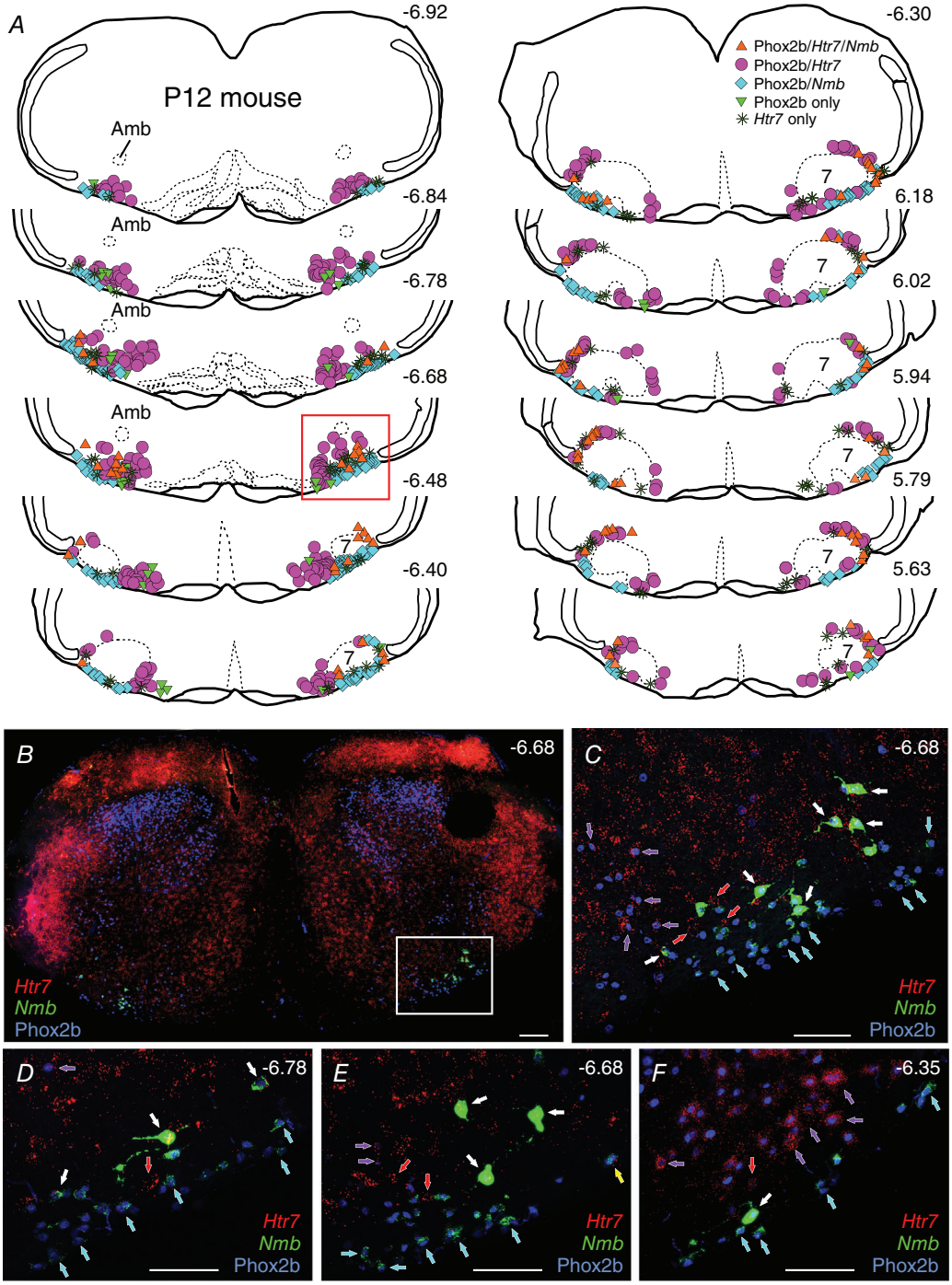

Figure 2. *Htr7* expression in parafacial region: RTN and other Phox2b+ neurons
A, multiplex RNAscope *in situ* hybridization for *Htr7* and *Nmb* was combined with immunostaining for Phox2b, and differentially labelled cells were mapped in sections through the parafacial region of P12 mouse brainstem, as indicated. For this and following figures, the distances from bregma in P12 mice were estimated based on anatomical landmarks and referenced to the relevant level in adult mice (Franklin & Paxinos, 2013). 7, facial motor nucleus; Amb, nucleus ambiguus. For clarity, Phox2b/*Htr7* neurons located within the facial nucleus were not plotted. Representative of $N = 4$ mice. *B* and *C*, photomicrographs from *A* (−6.68 mm relative to bregma); *C* is expanded from boxed area in *B*. Arrows indicate cells expressing: white, Phox2b/*Htr7*/*Nmb*; purple, Phox2b/*Htr7*; cyan, Phox2b/*Nmb*; red, *Htr7* alone. *D–F*, representative photomicrographs from a different mouse at the indicated rostrocaudal levels (mm, relative to bregma). Arrows as in *C*. Scale bars: *B*, 200 μm; *C–F*, 100 μm. [Colour figure can be viewed at wileyonlinelibrary.com]

than for *Kcnk5* (Fig. 6*D–F*), in that the dorsally located, *Htr7*-expressing *Nmb*$^{+}$ neurons that wrapped around the facial motor nucleus were typically devoid of *Gpr4* expression but occasionally expressed *Kcnk5*. Conversely, the main group of *Nmb*-expressing RTN neurons clustered closer to the ventral medullary surface and ventral to the facial motor nucleus, especially the *Nmb*-low cells, had higher levels of *Gpr4* and *Kcnk5* expression, and only low to undetectable levels of *Htr7* expression. This general co-expression pattern was also seen in adults, albeit again with lower overall expression levels of *Htr7* (Figs 7 and 8).

In summary, this cellular-level, molecular analysis indicates that *Htr7* is expressed in multiple Phox2b-expressing neurons in the parafacial region of the mouse brainstem, including but not limited to the RTN

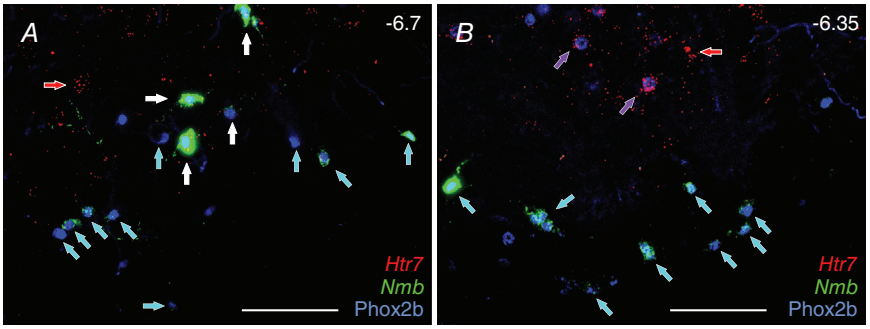

Figure 3. In adult mice, low levels of *Htr7* expression are associated with Phox2b-immunoreactive neurons, including in large *Nmb*-high cells
Multiplex RNAscope *in situ* hybridization for *Htr7* and *Nmb* was combined with immunostaining for Phox2b in adult mice (N = 4 mice), with representative images presented from caudal (*A*, −6.7 mm) and rostral (*B*, −6.35 mm) parafacial regions. Arrows indicate cells expressing: white, Phox2b/*Htr7*/*Nmb*; purple, Phox2b/*Htr7*; cyan, Phox2b/*Nmb*; red, *Htr7* alone. Distances relative to bregma; scale bars: 100 μm. [Colour figure can be viewed at wileyonlinelibrary.com]

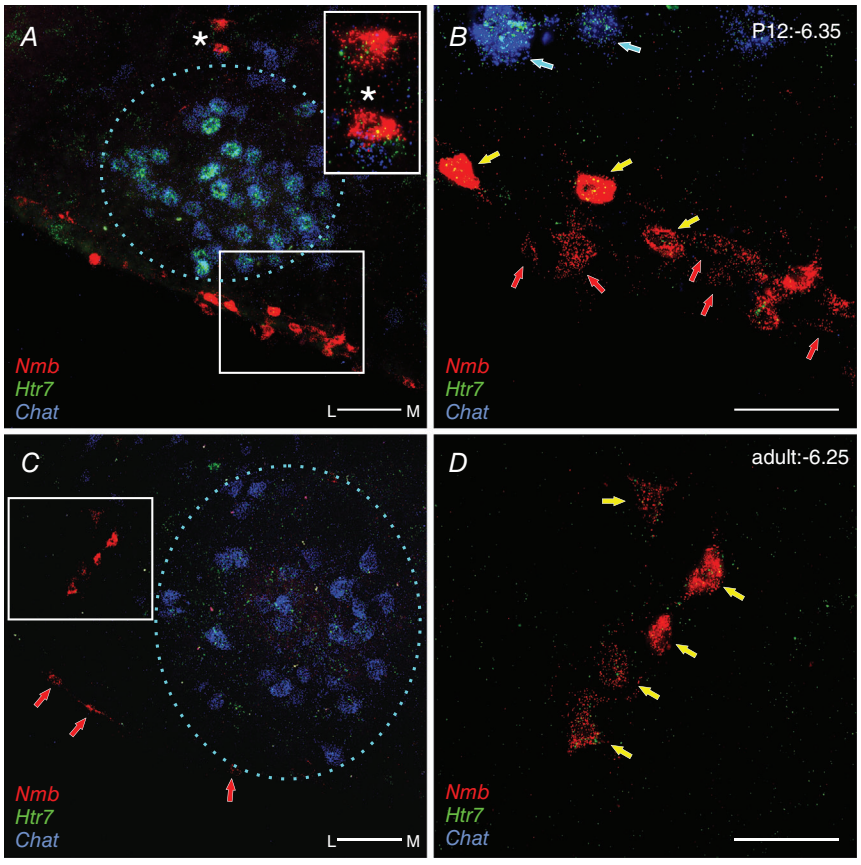

Figure 4. *Htr7* expression in *Chat*-expressing facial motoneurons
A–D, multiplex RNAscope *in situ* hybridization for *Htr7*, *Nmb* and *Chat* at the indicated rostrocaudal locations in young (P12, N = 4; *A*, *B*) and adult (P100, N = 4; *C*, *D*) mouse brainstem. *Inset* in *A* shows higher magnification of select neurons (denoted by *asterisks*); boxed regions (*A*, *C*) are expanded in higher power photomicrographs (*B*, *D*). Arrows indicate cells expressing: yellow, *Htr7*/*Nmb*; cyan, *Chat*/*Htr7*; red, *Nmb* alone; dashed lines encircle the facial nucleus. Scale bars: 100 μm: L, lateral: M, medial. [Colour figure can be viewed at wileyonlinelibrary.com]

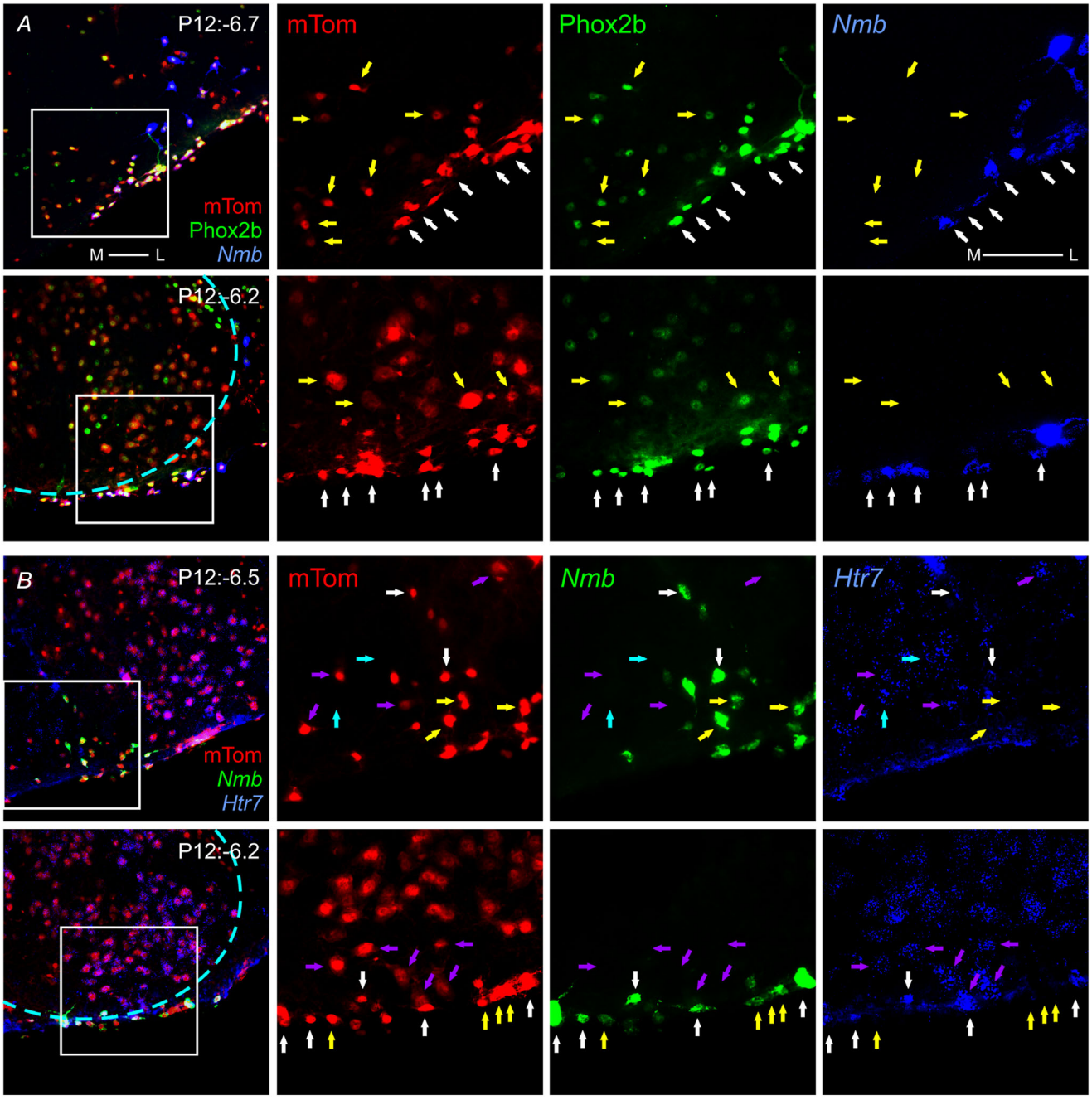

Figure 5. *Htr7* expression in RTN and non-RTN parafacial neurons labelled with a Phox2b-Cre dependent reporter
A, immunostaining for mTomato and Phox2b combined with RNAscope *in situ* hybridization for *Nmb* in ventral brainstem of P12 mouse at the indicated rostrocaudal levels (mm, relative to bregma). The boxed region in the colour overlay image (leftmost) is expanded for each of the markers, as indicated. Arrows indicate cells expressing: white, mTomato/Phox2b/*Nmb*; yellow, mTomato/Phox2b. Scale bars: 100 μm: L, lateral: M, medial. *B*, immunostaining for mTomato combined with RNAscope *in situ* hybridization for *Nmb* and *Htr7* in ventral brainstem of P12 mouse at the indicated rostrocaudal levels (mm, relative to bregma). The boxed region in the colour overlay image (leftmost) is expanded for each of the markers, as indicated. Arrows indicate cells expressing: white, mTomato/*Nmb*/*Htr7*; yellow, mTomato/*Nmb*; purple, mTomato/*Htr7*. Dashed lines delineate approximate boundaries of the facial nucleus; scale bars are 100 μm, with lateral (L) and medial (M) indicated. Representative of $N = 3$ mice. [Colour figure can be viewed at wileyonlinelibrary.com]

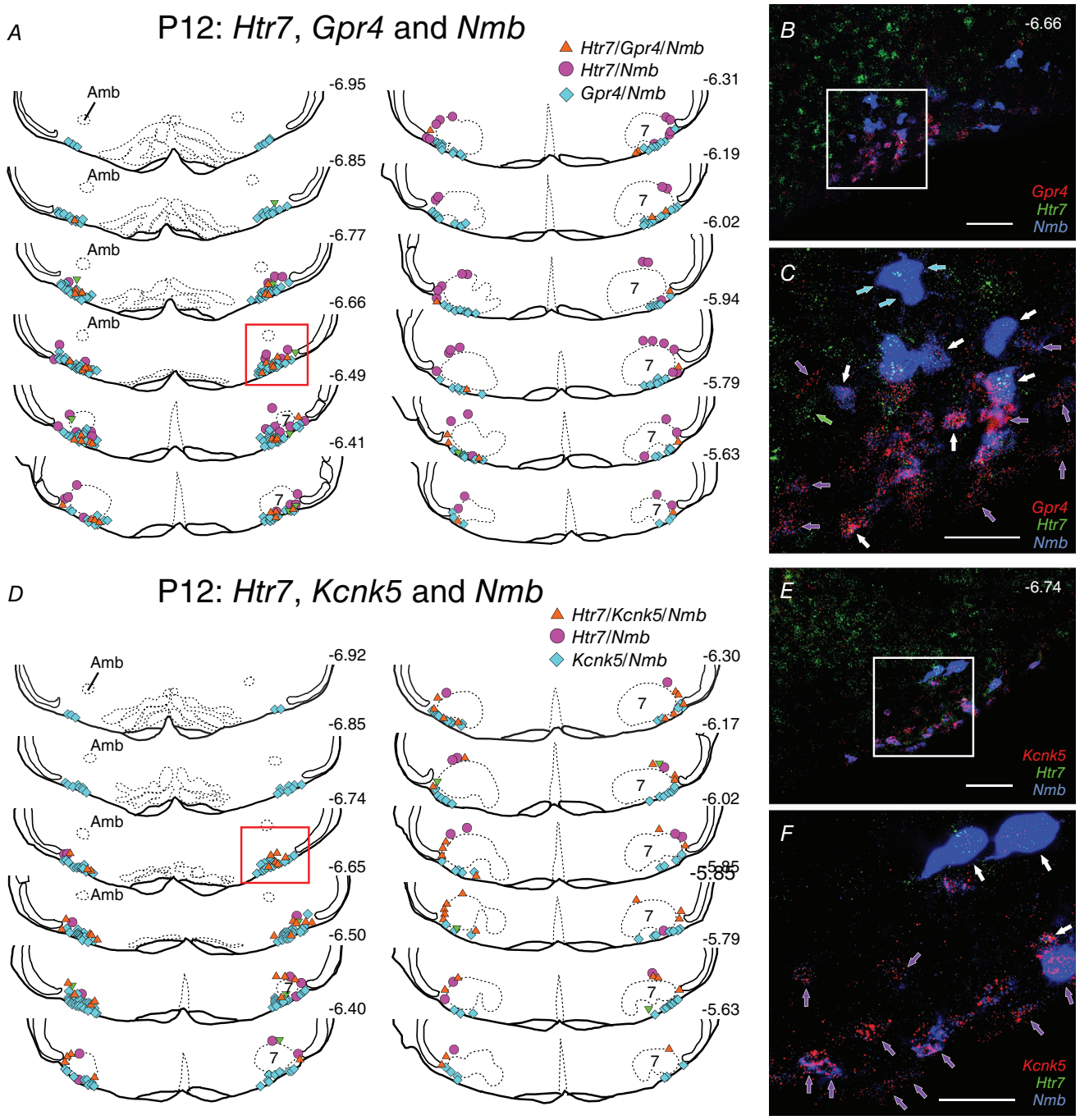

Figure 6. In young mice, *Htr7* expression is prominent in large, dorsally displaced *Nmb*-high neurons with low levels of *Gpr4* and *Kcnk5* expression
Multiplex RNAscope *in situ* hybridization for *Htr7*, *Nmb* and *Gpr4* (*A–C*) and for *Htr7*, *Nmb* and *Kcnk5* (*D–F*). *A* and *D*, labelled cells were mapped in sections through the parafacial region of P12 mouse brainstem at the indicated rostrocaudal levels. Representative of $N = 4$ mice. *B* and *C*, photomicrographs from *A* (−6.66 mm relative to bregma); *C* is expanded from boxed area in *B*, arrows indicate cells expressing: white, *Htr7*/*Gpr4*/*Nmb*; purple, *Gpr4*/*Nmb*; cyan, *Htr7*/*Nmb*; green, *Htr7* alone. *E* and *F*, photomicrographs from *D* (−6.74 mm relative to bregma); *F* is expanded from boxed area in *E*. Arrows indicate cells expressing: white, *Htr7*/*Kcnk5*/*Nmb*; purple, *Kcnk5*/*Nmb*. Scale bars: 100 μm. [Colour figure can be viewed at wileyonlinelibrary.com]

neurons defined by *Nmb* expression (Shi et al., 2017); many nearby neurons labelled in Phox2b-mTom reporter mice that are not bona fide *Nmb*-expressing RTN neurons also express *Htr7*. Among the RTN neurons, *Htr7* appears most prominently in the *Nmb*-high subgroup of large, dorsal RTN neurons that have low expression levels of the intrinsic proton detectors, *Gpr4* and *Kcnk5*; lower levels of *Htr7* expression are observed, albeit rarely, in the main cluster of RTN neurons located ventral to the facial motor nucleus and near the ventral medullary surface. A sharp decrease in *Htr7* expression is observed developmentally, with markedly lower levels observed throughout the adult brainstem.

CO_2 sensitivity of RTN neurons does not require 5-HT7 receptor function

Despite the limited expression of *Htr7* transcript in RTN neurons, previous evidence implicates 5-HT7 receptor actions in select electrophysiological effects of 5-HT

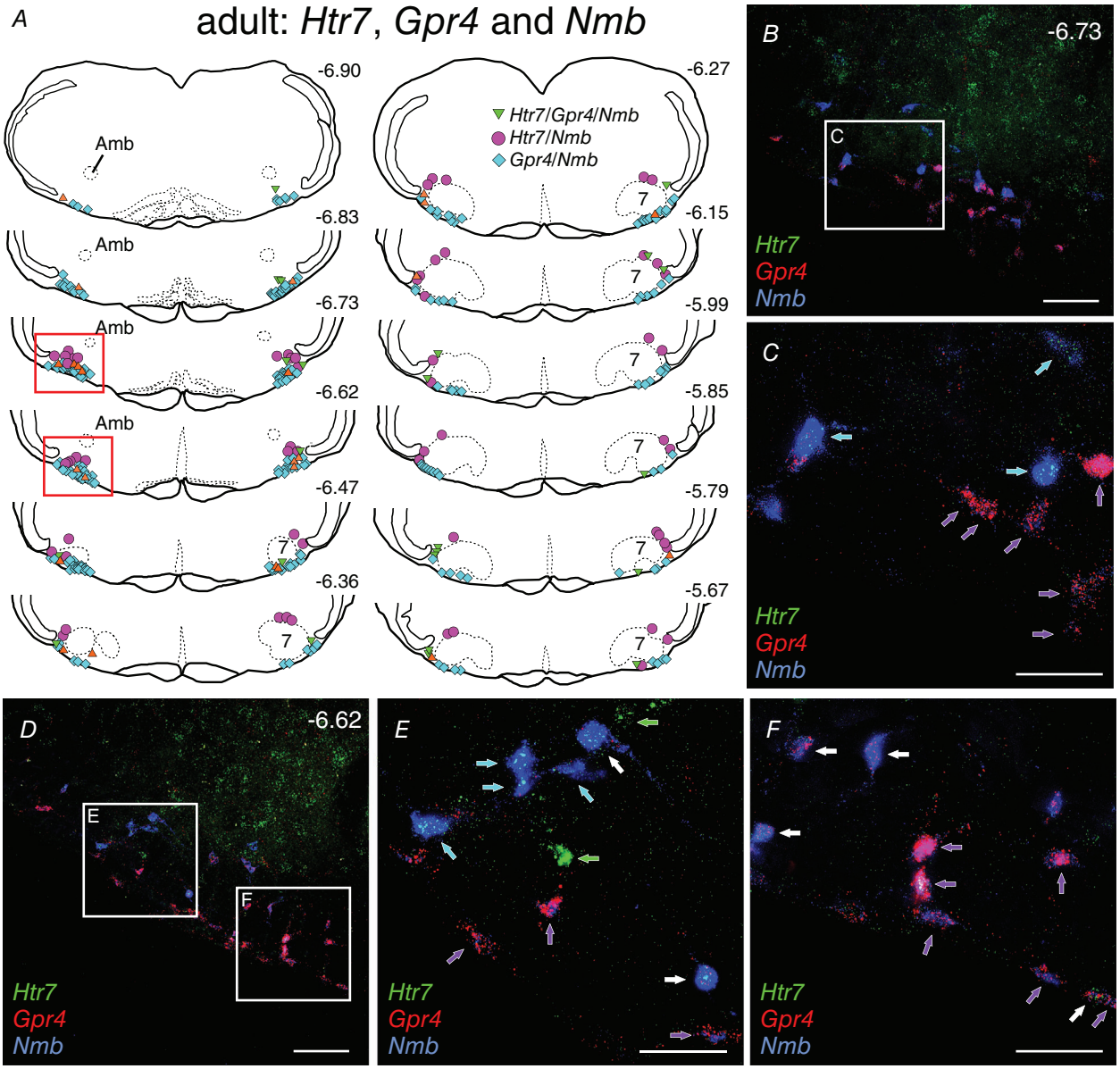

Figure 7. In adult mice, *Htr7* expression is typically found in *Gpr4*-negative, *Nmb*-high neurons
A, cells labelled by multiplex RNAscope *in situ* hybridization for *Htr7*, *Nmb* and *Gpr4* were mapped in sections through the parafacial region of adult mouse brainstem. Representative of $N = 4$ mice. *B–F*, photomicrographs from two different rostrocaudal levels (relative to bregma: *B* and *C*, −6.73 mm; *D–F*, −6.62 mm), with the boxed areas expanded as indicated. Arrows indicate cells expressing: white, *Htr7*/*Gpr4*/*Nmb*; purple, *Gpr4*/*Nmb*; cyan, *Htr7*/*Nmb*; green, *Htr7* alone. Scale bars: 100 μm. [Colour figure can be viewed at wileyonlinelibrary.com]

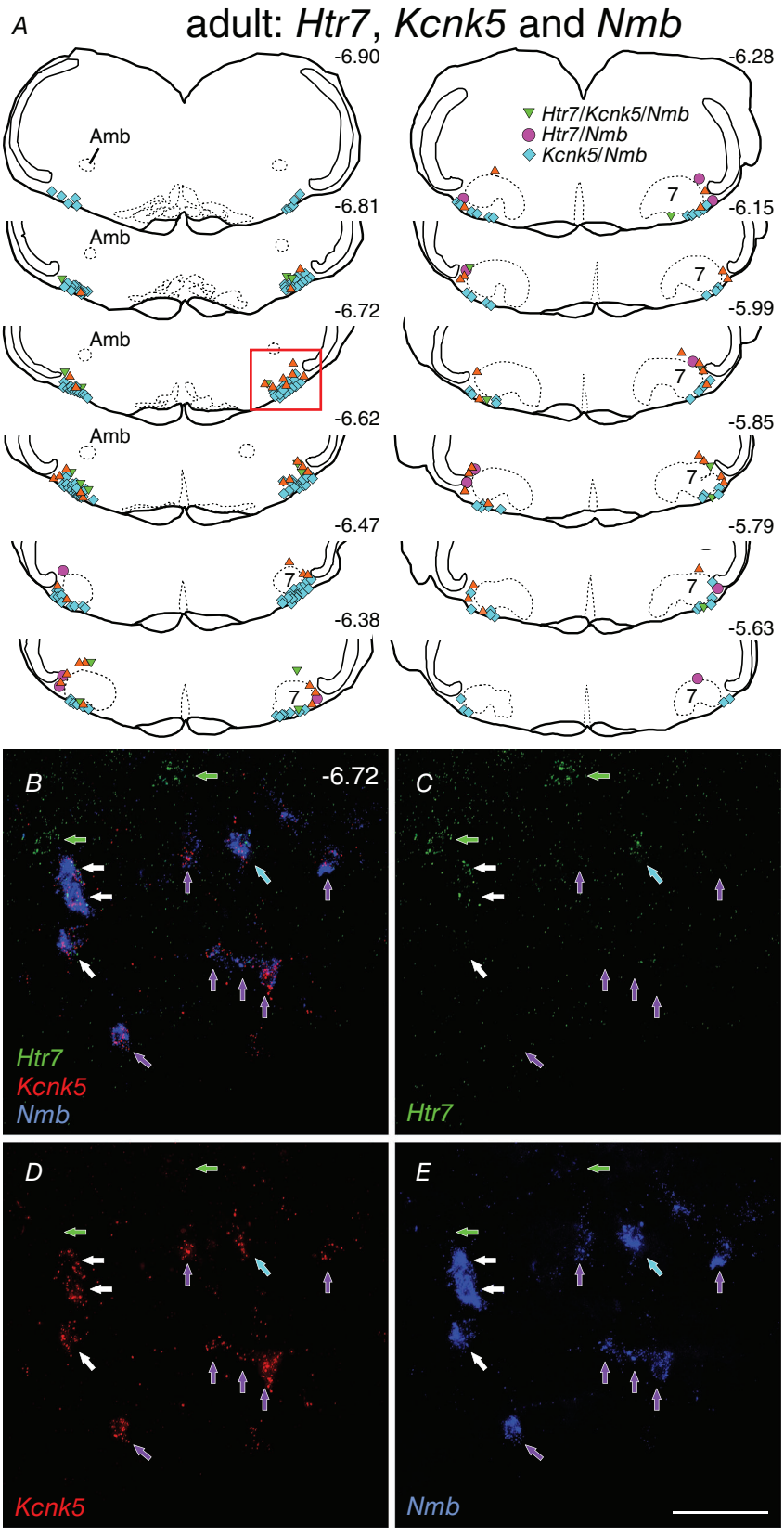

Figure 8. In adult mice, *Htr7* expressing *Nmb*-high neurons often co-express *Kcnk5* at low levels
A, cells labelled by multiplex RNAscope *in situ* hybridization for *Htr7*, *Nmb* and *Kcnk5* were mapped in sections through the parafacial region of adult mouse brainstem. Representative of $N = 4$ mice. *B–E*, photomicrographs (at −6.72 mm, relative to bregma) show merged image (*B*) and individual channels for *Htr7* (*C*), *Kcnk5* (*D*) and *Nmb* (*E*). Arrows indicate cells expressing: white, *Htr7*/*Kcnk5*/*Nmb*; purple, *Kcnk5*/*Nmb*; cyan, *Htr7*/*Nmb*; green, *Htr7* alone. Scale bar: 100 μm. [Colour figure can be viewed at wileyonlinelibrary.com]

(Hawkins et al., 2015; Wu et al., 2019) and provides a molecular underpinning for the recent suggestion that 5-HT7 receptor action may account for effects of CO_2/H^+ on RTN neurons (Wu et al., 2019). Therefore, as shown in Fig. 9, we revisited this latter suggestion by determining effects of a 5-HT7 receptor antagonist on the CO_2 and 5-HT responses from neurons in the parafacial region of brainstem slices from neonatal (P7–P12) Phox2b-mTom mice ($n = 7$, $N = 7$) or wild-type C57BL/6J mice ($n = 37$, $N = 37$). In all cases, recorded neurons were considered chemosensitive if they were spontaneously active under control conditions (5% CO_2; pH_o ~7.3) and responded to 10% CO_2 (pH_o ~7.0) with at least 1.0 Hz increase in firing (Fig. 9*A*–*C*). The baseline activity ($P = 0.13$) and firing responses to CO_2 ($P = 0.33$) were not different in chemosensitive neurons recorded from the two mouse lines (by unpaired *t*-test). We also confirmed that a subset of neurons identified in this manner were Phox2b-immunoreactive ($n = 7$), including some that were also mTomato$^+$ ($n = 4$), and verified

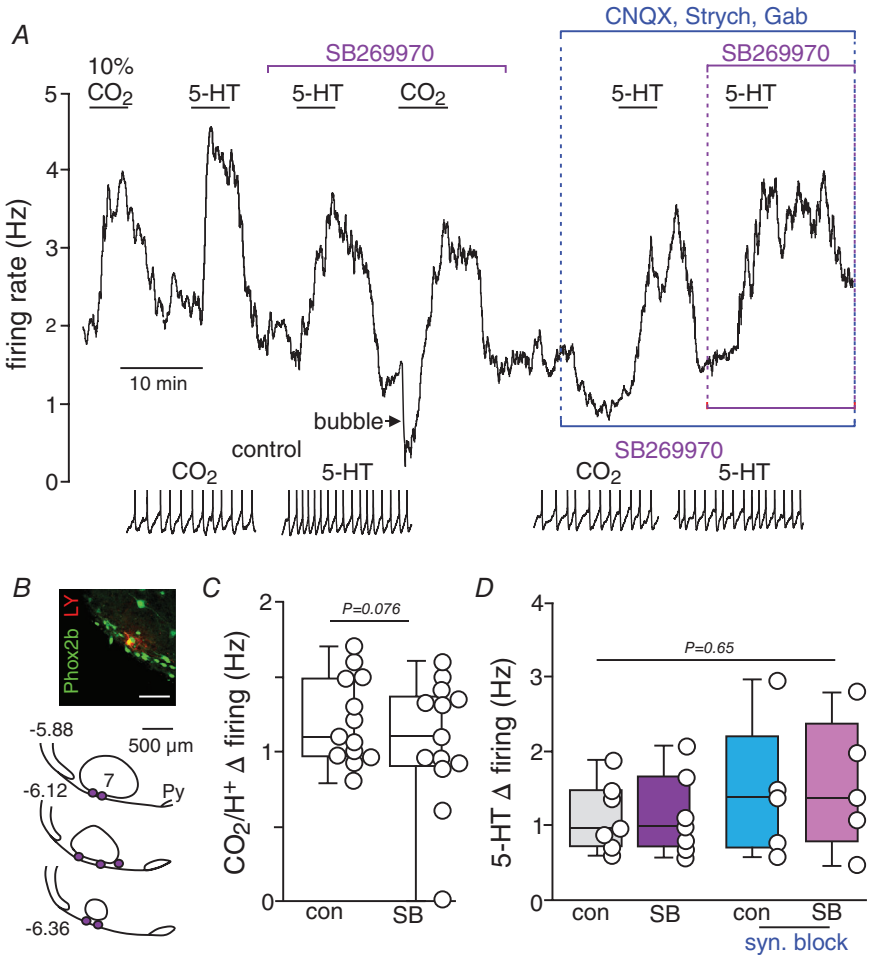

Figure 9. A 5-HT7 receptor blocker does not inhibit CO_2 responses of RTN neurons *in vitro*
A, trace of firing rate and segments of membrane potential (inset: spikes are truncated) show responses of a Phox2b$^+$ RTN neuron to 10 μM5-HT and 10% CO_2 under control conditions and in the presence of the 5-HT7 antagonist, SB269970 (10 μM), first in a standard bath solution and then in the presence of a synaptic blocker cocktail composed of CNQX (10 μM), strychnine (Strych; 2 μM) and gabazine (Gab; 10 μM). *B*, double-immunolabeling shows that a Lucifer Yellow (LY)-filled CO_2/H^+-sensitive RTN neuron (red) is immunoreactive for Phox2b (green). Scale bar: 75 μm. We confirmed that a subset of CO_2/H^+ activated RTN neurons ($n = 7$) were Phox2b-immunoreactive; computer-assisted plots show the relative location of these filled cells. Numbers to the left of each coronal section designate millimetres from bregma. 7, facial motor nucleus; Py, pyramidal tract. *C*, summary data (from $N = 13$ mice, one cell/slice/mouse) show firing response of RTN neurons to 10% CO_2 (Δ Hz) in control conditions and in the presence of SB269970 ($P = 0.076$, paired *t*-test). *D*, summary data ($N = 7$ mice, one cell/slice/mouse) show effects of 5-HT (10 μM) on firing activity of RTN neurons under control conditions and in the presence of SB269970 (10 μM), alone or with the synaptic blocker cocktail (one-way ANOVA; $P = 0.65$). [Colour figure can be viewed at wileyonlinelibrary.com]

their location ventral to the facial nucleus (Fig. 9*B*). The recorded neurons showed an average baseline activity of 2.1 ± 1.6 Hz (n = 13) and increased their discharge by 1.2 ± 0.3 Hz in response to 10% CO_2 under control conditions (Fig. 9*A* and *C*). A second exposure to 10% CO_2, this time when 5-HT7 receptors were blocked with 10 μM SB269970 (Di Pilato et al., 2014; Romero et al., 2006), increased activity by 1.1 ± 0.4 Hz (Fig. 9*A* and *C*); the CO_2-evoked change in firing was thus essentially identical between SB269970 and control conditions (P = 0.076, paired t-test). There was no effect of SB269970 on baseline firing frequency in these neurons (control, 1.9 ± 1.4 Hz *vs*. SB269970, 1.9 ± 1.4 Hz, n = 13; P = 0.61, by paired t-test). Also, contrary to evidence that 5-HT7 receptors regulate activity of RTN neurons (Hawkins et al., 2015; Wu et al., 2019), we found that SB269970 did not blunt firing responses to 5-HT (10 μM) at room temperature (22°C) (Fig. 9*D*; Δ Hz: 1.1 ± 0.5 Hz *vs*. 1.1 ± 0.6 Hz in 5-HT and 5-HT + SB269970; n = 7, P = 0.65, by one-way ANOVA), near body temperature (37°C, Δ Hz: 1.1 ± 0.6 Hz *vs*. 1.9 ± 0.9 at 22°C and 37°C; n = 5, P = 0.2, by unpaired t-test, not shown) or in the presence of a cocktail of fast neurotransmitter receptor blockers (Fig. 9*A* and *D*; Δ Hz in synaptic blocker cocktail: 5-HT = 1.5 ± 0.9 Hz *vs*. 1.6 ± 0.9 Hz in 5-HT and 5-HT + SB269970; n = 5, P = 0.65, by one-way ANOVA). Moreover, we found that LP-44 (2 μM), a 5-HT7 agonist, increased firing only modestly and only in ∼37% of the neurons tested (Δ Hz: 0.4 ± 0.1 Hz, P < 0.0001, by paired t-test; n = 7/19) most of the remaining neurons were unaffected by LP-44 (∼47%, n = 9/19) while a few were inhibited (∼16%, n = 3/19). This result is consistent with the low level of *Htr7* expression we observed in only a minor population of RTN neurons. However, in contrast to these more common observations in the majority of RTN neurons, we did encounter two cells for which the CO_2 response was reduced in the presence of SB269970 (not shown). Overall, these data indicate that the CO_2/H^+-sensitivity of most RTN neurons does not require 5-HT7 receptor signalling, the majority of which show little to no 5-HT7-mediated effects *in vitro*.

CO_2-stimulated breathing does not require 5-HT7 receptor signalling in the RTN

We next tested whether the ventilatory response to CO_2 requires intact 5-HT7 receptor activity in the RTN (Fig. 10). To localize effects to the RTN, we microinjected a 5-HT7 agonist and antagonist directly into the RTN region while performing whole body plethysmography in conscious adult mice (N = 7). All RTN injections were placed 100 μm below the facial motor nucleus and 200 μm rostral to the caudal end of the facial nucleus to target the region containing the highest density of CO_2-sensitive RTN neurons (Shi et al., 2017). An initial unilateral injection of the 5-HT7 receptor agonist LP-44 (2 mM, 50 nl; 100 pmol) (Di Pilato et al., 2014; Leopoldo et al., 2004) into the RTN elicited a clear increase in ventilation ($\dot{V}_E$, μl min^{-1} g^{-1}), with contributions from elevated respiratory frequency (f_R, breaths min^{-1}) and tidal volume (V_T, μl/breath g^{-1}) (Fig. 10*A*–*C*). Saline injections at the same site had no effect, and the LP-44-induced respiratory stimulation was completely blocked 10 min after pre-treatment with a bilateral injection of the 5-HT7 receptor antagonist, SB269970 (1 mM, 50 nl; 50 pmol). Importantly, this internal control indicates that SB269970 was provided at a functionally relevant location and concentration. We then examined effects of CO_2 on breathing before and 10 min. after bilateral injection of SB269970 at the same sites in these mice. We found that increasing inspired concentrations of CO_2 (F_{iCO_2} = 0.02–0.1) elicited essentially identical changes in f_R, V_T and $\dot{V}_E$ before and after administration of the 5-HT7 receptor blocker (Fig. 10*D*–*F*). Histological examination of injection sites verified that the tip of the injection cannula was located within the RTN (Fig. 10*G*). These data indicate that 5-HT7 receptor stimulation in the region of the RTN can increase ventilation, but 5-HT7 receptor activation is not required for CO_2-stimulated breathing.

Discussion

In this study, we examined the parafacial region of the mouse brainstem for the distribution and function of 5-HT7 receptors. This receptor subtype was proposed to mediate, at least in part, the effects of 5-HT on RTN neurons (Hawkins et al., 2015; Wu et al., 2019) and suggested to account, in the main, for RTN neuronal CO_2/H^+ sensitivity (Wu et al., 2019). We found that 5-HT7 receptor transcripts are indeed detectable in a relatively small subpopulation of *Nmb*-positive RTN respiratory chemoreceptors, albeit with diminishing expression from the early postnatal to the adult period. In addition, although injection of 5-HT7 agonists into the RTN region could stimulate breathing, we found that neither the cellular (increased action potential firing) nor the integrative (increased breathing) response to CO_2 was affected by blocking 5-HT7 receptors in the RTN. Collectively, these data are consistent with a contribution to breathing of 5-HT7 receptor signalling in the parafacial region, perhaps via some minor actions on RTN neurons as suggested from earlier work (Hawkins et al., 2015; Wu et al., 2019). However, they do not support the recent suggestion that 5-HT7 receptors account for a major component of the CO_2/H^+ sensitivity of RTN respiratory chemoreceptor neurons and for their effect on CO_2-stimulated breathing (Wu et al., 2019).

The pattern of 5-HT7 receptor expression does not support a role in RTN neuronal CO_2/H^+ sensitivity or CO_2-regulated breathing

Several observations with respect to the 5-HT7 receptor expression profile in the ventral parafacial brainstem region are incompatible with known properties of CO_2/H^+ sensitivity of RTN neurons and central respiratory chemosensitivity. First, it is well known that the overall sensitivity of the respiratory system to CO_2 increases during development (Cerpa et al., 2017; Hodges & Richerson, 2010; Putnam et al., 2005). However, this developmental increase in effects of CO_2 on breathing runs opposite to *Htr7* expression levels, which are at higher levels during the early postnatal period and decrease to lower levels in the adult throughout the brainstem, including in the RTN. We also noted that *Htr7* is low or undetectable in most *Nmb*-expressing RTN neurons located ventral to the facial nucleus, the principal group of putative CO_2/H^+ chemosensory neurons (Shi et al., 2017). This was evident across three different assay systems: single cell RNA-Seq, multiplex single cell qRT-PCR, and RNAscope *in situ* hybridization. Although each approach presents some specific limitations (see below), the general convergence of results from these complementary experiments inspires some confidence that 5-HT7 receptor expression is indeed low in the RTN neurons associated with central respiratory chemosensitivity. Notably, *Htr7* expression was consistently found in fewer RTN neurons and at lower levels than either *Kcnk5* or *Gpr4*, which encode the two proton detectors implicated in the intrinsic CO_2/H^+ sensitivity of RTN neurons (Gestreau et al., 2010; Kumar et al., 2015; Wang, Benamer et al., 2013). Finally, the RTN neurons most likely to express detectable levels of *Htr7* were a distinct group of *Nmb*-high cells that do not appear to be chemosensitive, as judged by the absence of *Fos* induction after CO_2 exposure *in vivo* (Shi et al., 2017). It is possible

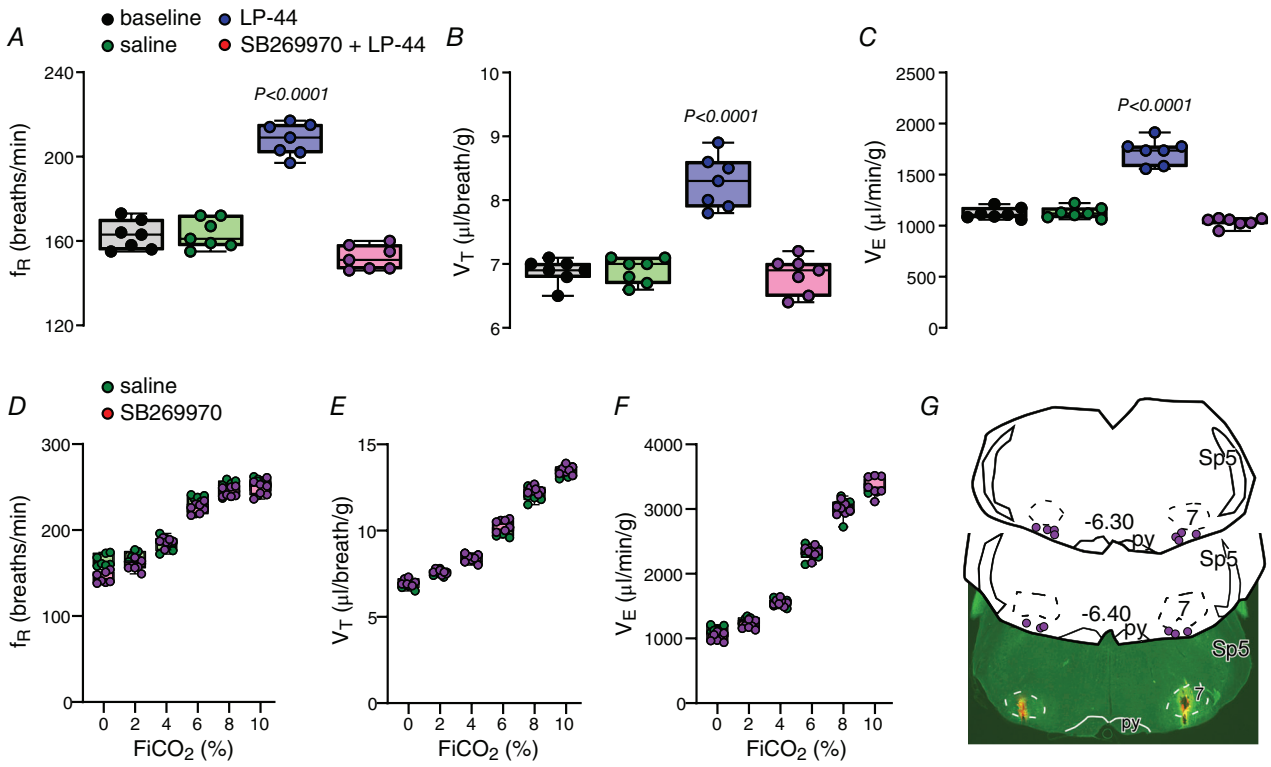

Figure 10. A 5-HT7 receptor blocker in RTN does not affect CO_2-stimulated breathing *in vivo*
The effect of local microinjection into the RTN of 5-HT7 receptor agonist (LP-44, 2 mM, 50 nl; 100 pmol) and antagonist (SB269970, 1 mM, 50 nl; 50 pmol) on respiratory frequency (*A* and *D*: f_R, breaths min^{-1}), tidal volume (*B* and *E*: V_T, μl breath^{-1} g^{-1}) and their product, minute ventilation (*C* and *F*: $\dot{V}_E$, μl min^{-1} g^{-1}) measured by whole body plethysmography in conscious mice (N = 7) under baseline conditions (*A*–*C*) and during exposure to increasing concentrations of ambient CO_2 (0–10% CO_2, balance O_2) after bilateral injections of saline or SB269970 (1 mM, 50 nl; 50 pmol) into the RTN (*D*–*F*). The LP-44-evoked stimulation of breathing ($*P < 0.0001$) was blocked by SB269970; despite this, SB269970 had no effect on CO_2-stimulated breathing (P = 0.224, by two-way RM ANOVA). *G*, photomicrograph showing the location of an exemplar bilateral microinjection into the RTN, and schematic drawings (bregma levels: −6.3 and −6.4 mm) depicting the location of all microinjections into the RTN (N = 7). 7, facial motor nucleus; Py, pyramidal tract; Sp5, spinal trigeminal nucleus. [Colour figure can be viewed at wileyonlinelibrary.com]

that these *Nmb*-high cells are a subset of RTN neurons that are particularly sensitive to 5-HT7-mediated modulation and participate in some other breathing functions, such as sighing (Li et al., 2016); we note, however, that we did not observe any differences in sigh frequency after LP-44 injection into the RTN. Overall, *Htr7* expression in RTN neurons appears to be a poor match to account for CO_2/H^+ sensitivity of RTN neurons.

5-HT7R activity in the RTN is dispensable for CO_2/H^+ sensitivity at the cellular and whole animal levels

Expression levels for receptor transcripts, or even the receptor itself, may be imprecise predictors of receptor function. Therefore, we also tested effects of specific 5-HT7 receptor compounds on RTN neuronal function, *in vitro* and *in vivo*. Those functional experiments generally provided no evidence for the hypothesized contributions of 5-HT7 receptors to CO_2/H^+ sensitivity of RTN neurons or RTN-mediated central respiratory chemosensitivity.

First, we recorded effects of the 5-HT7 receptor blocker SB269970 on CO_2-responsive RTN neurons in brainstem slices from wild-type mice. In all but two of these cells (n = 11/13), we found that SB269970 had negligible effects on CO_2-evoked stimulation of firing. These data stand in contrast to recent observations on presumptive RTN neurons, recorded in brain slices and in dissociated culture, for which the same 5-HT7 blocker at the same concentration nearly eliminated CO_2-evoked changes in firing (decreased by 63−92%) (Wu et al., 2019). The reasons for these discrepancies are unclear. As acknowledged (Wu et al., 2019), it is possible that the earlier recordings were made from cells other than RTN neurons. In that work, recorded cells were identified in Phox2b::Cre mice based on expression of a Cre-dependent mTomato fluorescent reporter (Wu et al., 2019). As we demonstrate here, this approach can identify bona fide Nmb^+ RTN neurons that universally express Phox2b (Shi et al., 2017; Stornetta et al., 2006), but it will also mark other non-RTN cells. Expression of Phox2b is not limited to RTN neurons in the parafacial region (Stornetta et al., 2006) and we show here that *Htr7* expression is localized to many neurons that are Phox2b-immunoreactive and/or express a Phox2b-Cre-dependent mTomato reporter, but which are not actually RTN neurons (i.e. they do not express *Nmb*). In addition, Cre-dependent reporter gene expression can also occur in non-Phox2b cells due to ephemeral or even ectopic expression of Cre in this BAC transgenic mouse line (Czeisler et al., 2019). These issues would be most pronounced in the earlier cell culture studies, in which anatomical landmarks were no longer available, but they should be mitigated in slice preparations for which targeting the appropriate parafacial region is more straightforward. Indeed, and consistent with the paucity of *Htr7* expression in RTN neurons, we found that SB269970 had no effect on CO_2 responses localized within the main cluster of RTN neurons ventral to the facial nucleus. In this respect, it is worth noting that the plotted location of cells recorded in slices from that previous work (see Fig. 3 from Wu et al., 2019) was decidedly dorsomedial to the main cluster of RTN neurons and thus appeared to overlap with the location of a substantial group of *Htr7*-expressing, Phox2b-positive neurons that we found outside the RTN (i.e. *Nmb*-negative: see magenta circles in Fig. 2*A*, purple arrows in Fig. 2*C*).

We also examined effects of 5-HT7 receptor function in the RTN on CO_2-stimulated breathing in conscious mice. Whereas microinjection of SB269970 directly into the RTN blocked effects of the co-injected 5-HT7 agonist LP-44, demonstrating effective 5-HT7 receptor inhibition, it had no effect on CO_2-stimulated breathing. These data compellingly dispute earlier conclusions, and warrant examination of potentially salient methodological differences. In that previous work, a more broad-spectrum 5-HT2/7 antagonist (ketanserin) was administered systemically in mice (Wu et al., 2019), and thus it may have acted on other 5-HT receptors and/or at other raphe target sites. Indeed, it is well known that 5-HT has general facilitatory effects on motor output, including breathing (Brust et al., 2014; Jacobs et al., 2002), and the reported blunting of CO_2-stimulated breathing by systemic ketanserin is consistent with those known actions. So, unlike our work, those earlier *in vivo* experiments do not address 5-HT7 receptor actions specifically in the RTN region; they also cannot be interpreted unambiguously in terms of 5-HT7 receptor contributions to CO_2/H^+ sensitivity of RTN neurons or RTN-mediated central respiratory chemosensitivity.

Caveats and experimental limitations

Our single cell molecular approaches relied on visualizing and harvesting individual GFP-labelled neurons from the RTN region of brainstem slices for quantitative analysis of *Htr7* expression selectively in *Nmb*-positive cells (i.e. RTN neurons) (Shi et al., 2017). It is not possible to exclude some selection bias with this manual cell picking. This concern was allayed by the addition of RNAscope multiplex *in situ* hybridization assays, which assessed *Htr7* expression across the entire parafacial region and in neurons expressing *Nmb* and other relevant markers (e.g. Phox2b, *Chat*, *Gpr4*, *Kcnk5*) (Shi et al., 2017). Although previous scRNA-seq data are highly quantitative (Shi et al., 2017), expression levels determined here by sc-qPCR and RNAscope should be considered semi-quantitative, especially when comparing across gene transcripts. Also, detection thresholds may vary between cells, and lack

of detection cannot necessarily be equated with lack of expression. Nonetheless, these complementary analyses all lead to the same conclusion: *Htr7* transcripts are found in only a minor subset of RTN neurons (∼20–50%), and then at levels lower than *Gpr4* and *Kcnk5*.

To address the experimental limitation that our molecular assessment was based on measures of *Htr7* transcripts, and not on functional 5-HT7 receptor protein, we used selective receptor pharmacology and electrophysiological recordings in the RTN to assess 5-HT7 receptor contributions to CO_2/H^+ sensitivity in presumptive RTN neurons. The recorded cells were all located in the ventral parafacial region of brainstem slices, either from wild-type mice or targeted based on mTomato expression in Phox2b-mTom mice; in addition, we confirmed that a subset of cells identified in this manner were also Phox2b-immunoreactive. Moreover, these cells were functionally characterized as chemosensitive neurons by their increased firing response to elevated CO_2/H^+ (Hawkins et al., 2015; Hawryluk et al., 2012). Together, we believe this cell selection approach reliably identified bona fide RTN neurons. The ventrally located parafacial cells we recorded were found within the major cluster of RTN neurons, a group of cells that show little, if any, *Htr7* expression. Even so, these RTN neurons were clearly responsive to changes in CO_2/H^+, and their chemosensitivity was not dependent on 5-HT7 receptor signalling. At present, we do not have a method to specifically target the *Nmb*-high subpopulation of RTN neurons that more reliably express *Htr7* and lower levels of *Gpr4*/*Kcnk5*. This *Nmb*-high subset of RTN neurons does not express Fos after CO_2 exposure *in vivo* (Shi et al., 2017). However, it remains possible that *Nmb*-high cells may be CO_2/H^+-sensitive when examined *in vitro*, and that chemosensitivity in that minor group of cells could be 5-HT7-dependent. We also note that electrophysiological recordings were performed in slices from neonates and studies of CO_2-stimulated breathing were performed in adults; nevertheless, we found no effect of 5-HT7 compounds at either age and, importantly, our direct recordings of RTN chemosensitivity were obtained in neonates when *Htr7* levels were highest.

We also used receptor pharmacology and local RTN microinjection *in vivo* to test the purported contributions of 5-HT7 receptors to breathing and respiratory chemosensitivity in conscious adult mice. Although the compounds we employed are considered specific for 5-HT7 receptors (Di Pilato et al., 2014), an unavoidable concern with such pharmacological studies is potential off-target effects on other receptors or on other cells. For example, we found that injection of the 5-HT7 agonist LP-44 into the RTN region stimulated breathing, an effect that may be due to either activation of the *Htr7*-expressing subset of RTN neurons or actions of the injectate on other *Htr7*-expressing cells located nearby or in adjacent regions. Regardless, the 5-HT7 antagonist SB269970 clearly blocked local 5-HT7 actions of LP-44, and any non-specific actions of the antagonist were also without effect on CO_2-stimulated breathing. It is conceivable that a cell-specific genetic approach could more selectively target 5-HT7 receptors in RTN neurons. However, those approaches are subject to their own issues (e.g. homeostatic compensation), and respiratory deficits have not been listed among the defects in global 5-HT7 knockout mice and rats (Demireva et al., 2019; Hedlund et al., 2003; Matthys et al., 2011). Finally, we note that although our experiments were performed on awake mice, they were conducted during the inactive daytime period when serotonergic systems are also less active (Hodges & Richerson, 2010; Jacobs et al., 2002). Therefore, even though CO_2-stimulated breathing was robust under these conditions, it is possible that serotonin signalling via 5-HT7 receptors could make some more substantial contributions under different conditions.

In conclusion, none of these shortcomings obtend our major conclusions that 5-HT7 receptor activation in the RTN is not required for either RTN neuron chemosensitivity or RTN neuron-mediated contributions to CO_2-stimulated breathing.

References

Basting, T. M., Burke, P. G., Kanbar, R., Viar, K. E., Stornetta, D. S., Stornetta, R. L., & Guyenet, P. G. (2015). Hypoxia silences retrotrapezoid nucleus respiratory chemoreceptors via alkalosis. *Journal of Neuroscience*, **35**, 527–543.

Brust, R. D., Corcoran, A. E., Richerson, G. B., Nattie, E., & Dymecki, S. M. (2014). Functional and developmental identification of a molecular subtype of brain serotonergic neuron specialized to regulate breathing dynamics. *Cell Reports*, **9**, 2152–2165.

Cerpa, V. J., Wu, Y., Bravo, E., Teran, F. A., Flynn, R. S., & Richerson, G. B. (2017). Medullary 5-HT neurons: Switch from tonic respiratory drive to chemoreception during postnatal development. *Neuroscience*, **344**, 1–14.

Cleary, C. M., Milla, B. M., Kuo, F. S., James, S., Flynn, W. F., Robson, P., & Mulkey, D. K. (2021). Somatostatin-expressing parafacial neurons are $CO_2/H(+)$ sensitive and regulate baseline breathing. *eLife*, **10**, e60317.

Czeisler, C. M., Silva, T. M., Fair, S. R., Liu, J., Tupal, S., Kaya, B., Cowgill, A., Mahajan, S., Silva, P. E., Wang, Y., Blissett, A. R., Goksel, M., Borniger, J. C., Zhang, N., Fernandes-Junior, S. A., Catacutan, F., Alves, M. J., Nelson, R. J., Sundaresean, V., … Otero, J. J. (2019). The role of PHOX2B-derived astrocytes in chemosensory control of breathing and sleep homeostasis. *Journal of Physiology*, **597**, 2225–2251.

Del Negro, C. A., Funk, G. D., & Feldman, J. L. (2018). Breathing matters. *Nature Reviews. Neuroscience*, **19**, 351–367.

Demireva, E. Y., Xie, H., Flood, E. D., Thompson, J. M., Seitz, B. M., & Watts, S. W. (2019). Creation of the 5-hydroxytryptamine receptor 7 knockout rat as a tool for cardiovascular research. *Physiological Genomics*, **51**, 290–301.

Di Pilato, P., Niso, M., Adriani, W., Romano, E., Travaglini, D., Berardi, F., Colabufo, N. A., Perrone, R., Laviola, G., Lacivita, E., & Leopoldo, M. (2014). Selective agonists for serotonin 7 (5-HT7) receptor and their applications in preclinical models: An overview. *Reviews in the Neurosciences*, **25**, 401–415.

Drorbaugh, J. E., & Fenn, W. O. (1955). A barometric method for measuring ventilation in newborn infants. *Pediatrics*, **16**, 81–87.

Dubreuil, V., Ramanantsoa, N., Trochet, D., Vaubourg, V., Amiel, J., Gallego, J., Brunet, J. F., & Goridis, C. (2008). A human mutation in Phox2b causes lack of CO_2 chemosensitivity, fatal central apnea, and specific loss of parafacial neurons. *Proceedings of the National Academy of Sciences, USA*, **105**, 1067–1072.

Dubreuil, V., Thoby-Brisson, M., Rallu, M., Persson, K., Pattyn, A., Birchmeier, C., Brunet, J. F., Fortin, G., & Goridis, C. (2009). Defective respiratory rhythmogenesis and loss of central chemosensitivity in Phox2b mutants targeting retrotrapezoid nucleus neurons. *Journal of Neuroscience*, **29**, 14836-14846.

Feldman, J. L., Mitchell, G. S., & Nattie, E. E. (2003). Breathing: Rhythmicity, plasticity, chemosensitivity. *Annual Review of Neuroscience*, **26**, 239–266.

Franklin, K. B. J., & Paxinos, G. (2013). *Paxinos and Franklin's the mouse brain in stereotaxic coordinates*. Academic Press.

Gestreau, C., Heitzmann, D., Thomas, J., Dubreuil, V., Bandulik, S., Reichold, M., Bendahhou, S., Pierson, P., Sterner, C., Peyronnet-Roux, J., Benfriha, C., Tegtmeier, I., Ehnes, H., Georgieff, M., Lesage, F., Brunet, J. F., Goridis, C., Warth, R., & Barhanin, J. (2010). Task2 potassium channels set central respiratory CO_2 and O_2 sensitivity. *Proceedings of the National Academy of Sciences, USA*, **107**, 2325–2330.

Gourine, A. V., Kasymov, V., Marina, N., Tang, F., Figueiredo, M. F., Lane, S., Teschemacher, A. G., Spyer, K. M., Deisseroth, K., & Kasparov, S. (2010). Astrocytes control breathing through pH-dependent release of ATP. *Science*, **329**, 571–575.

Gourine, A. V., Llaudet, E., Dale, N., & Spyer, K. M. (2005). ATP is a mediator of chemosensory transduction in the central nervous system. *Nature*, **436**, 108–111.

Guyenet, P. G., & Bayliss, D. A. (2015). Neural control of breathing and CO_2 homeostasis. *Neuron*, **87**, 946–961.

Guyenet, P. G., Stornetta, R. L., Souza, G., Abbott, S. B. G., Shi, Y., & Bayliss, D. A. (2019). The retrotrapezoid nucleus: Central chemoreceptor and regulator of breathing automaticity. *Trends in Neuroscience*, **42**, 807–824.

Hagan, J. J., Price, G. W., Jeffrey, P., Deeks, N. J., Stean, T., Piper, D., Smith, M. I., Upton, N., Medhurst, A. D., Middlemiss, D. N., Riley, G. J., Lovell, P. J., Bromidge, S. M., & Thomas, D. R. (2000). Characterization of SB-269970-A, a selective 5-HT(7) receptor antagonist. *British Journal of Pharmacology*, **130**, 539–548.

Haldane, J. S., & Priestley, J. G. (1905). The regulation of the lung-ventilation. *Journal of Physiology*, **32**, 225–266.

Hawkins, V. E., Hawryluk, J. M., Takakura, A. C., Tzingounis, A. V., Moreira, T. S., & Mulkey, D. K. (2015). HCN channels contribute to serotonergic modulation of ventral surface chemosensitive neurons and respiratory activity. *Journal of Neurophysiology*, **113**, 1195–1205.

Hawryluk, J. M., Moreira, T. S., Takakura, A. C., Wenker, I. C., Tzingounis, A. V., & Mulkey, D. K. (2012). KCNQ channels determine serotonergic modulation of ventral surface chemoreceptors and respiratory drive. *Journal of Neuroscience*, **32**, 16943–16952.

Hedlund, P. B., Danielson, P. E., Thomas, E. A., Slanina, K., Carson, M. J., & Sutcliffe, J. G. (2003). No hypothermic response to serotonin in 5-HT7 receptor knockout mice. *Proceedings of the National Academy of Sciences, USA*, **100**, 1375–1380.

Hodges, M. R., & Richerson, G. B. (2010). Medullary serotonin neurons and their roles in central respiratory chemoreception. *Respiratory Physiology & Neurobiology*, **173**, 256–263.

Jacobs, B. L., Martin-Cora, F. J., & Fornal, C. A. (2002). Activity of medullary serotonergic neurons in freely moving animals. *Brain Research Brain Research Reviews*, **40**, 45–52.

Kumar, N. N., Velic, A., Soliz, J., Shi, Y., Li, K., Wang, S., Weaver, J. L., Sen, J., Abbott, S. B., Lazarenko, R. M., Ludwig, M. G., Perez-Reyes, E., Mohebbi, N., Bettoni, C., Gassmann, M., Suply, T., Seuwen, K., Guyenet, P. G., Wagner, C. A., & Bayliss, D. A. (2015). Regulation of breathing by CO(2) requires the proton-activated receptor GPR4 in retrotrapezoid nucleus neurons. *Science*, **348**, 1255–1260.

Lazarenko, R. M., Milner, T. A., Depuy, S. D., Stornetta, R. L., West, G. H., Kievits, J. A., Bayliss, D. A., & Guyenet, P. G. (2009). Acid sensitivity and ultrastructure of the retrotrapezoid nucleus in Phox2b-EGFP transgenic mice. *Journal of Comparative Neurology*, **517**, 69–86.

Leopoldo, M., Berardi, F., Colabufo, N. A., Contino, M., Lacivita, E., Niso, M., Perrone, R., & Tortorella, V. (2004). Structure-affinity relationship study on N-(1,2,3,4-tetrahydronaphthalen-1-yl)-4-aryl-1-piperazinealkylamides, a new class of 5-hydroxytryptamine7 receptor agents. *Journal of Medicinal Chemistry*, **47**, 6616–6624.

Li, P., Janczewski, W. A., Yackle, K., Kam, K., Pagliardini, S., Krasnow, M. A., & Feldman, J. L. (2016). The peptidergic control circuit for sighing. *Nature*, **530**, 293–297.

Matthys, A., Haegeman, G., Van Craenenbroeck, K., & Vanhoenacker, P. (2011). Role of the 5-HT7 receptor in the central nervous system: From current status to future perspectives. *Molecular Neurobiology*, **43**, 228–253.

Mitchell, R. A., Loeschcke, H. H., Massion, W. H., & Severinghaus, J. W. (1963). Respiratory responses mediated through superficial chemosensitive areas on the medulla. *Journal of Applied Physiology*, **18**, 523–533.

Moreira, T. S., Sobrinho, C. R., Falquetto, B., Oliveira, L. M., Lima, J. D., Mulkey, D. K., & Takakura, A. C. (2021). The retrotrapezoid nucleus and the neuromodulation of breathing. *Journal of Neurophysiology*, **125**, 699–719.

Mulkey, D. K., Rosin, D. L., West, G., Takakura, A. C., Moreira, T. S., Bayliss, D. A., & Guyenet, P. G. (2007). Serotonergic neurons activate chemosensitive retrotrapezoid nucleus neurons by a pH-independent mechanism. *Journal of Neuroscience*, **27**, 14128–14138.

Mulkey, D. K., Stornetta, R. L., Weston, M. C., Simmons, J. R., Parker, A., Bayliss, D. A., & Guyenet, P. G. (2004). Respiratory control by ventral surface chemoreceptor neurons in rats. *Nature Neuroscience*, **7**, 1360–1369.

Pfaffl, M. W. (2001). A new mathematical model for relative quantification in real-time RT-PCR. *Nucleic Acids Research*, **29**, 45e.

Putnam, R. W., Conrad, S. C., Gdovin, M. J., Erlichman, J. S., & Leiter, J. C. (2005). Neonatal maturation of the hypercapnic ventilatory response and central neural CO_2 chemosensitivity. *Respiratory Physiology & Neurobiology*, **149**, 165–179.

Ramanantsoa, N., Hirsch, M. R., Thoby-Brisson, M., Dubreuil, V., Bouvier, J., Ruffault, P. L., Matrot, B., Fortin, G., Brunet, J. F., Gallego, J., & Goridis, C. (2011). Breathing without CO(2) chemosensitivity in conditional Phox2b mutants. *Journal of Neuroscience*, **31**, 12880–12888.

Romero, G., Pujol, M., & Pauwels, P. J. (2006). Reanalysis of constitutively active rat and human 5-HT7(a) receptors in HEK-293F cells demonstrates lack of silent properties for reported neutral antagonists. *Naunyn-Schmiedebergs Archives of Pharmacology*, **374**, 31–39.

Rossi, J., Balthasar, N., Olson, D., Scott, M., Berglund, E., Lee, C. E., Choi, M. J., Lauzon, D., Lowell, B. B., & Elmquist, J. K. (2011). Melanocortin-4 receptors expressed by cholinergic neurons regulate energy balance and glucose homeostasis. *Cell Metabolism*, **13**, 195–204.

Shi, Y., Abe, C., Holloway, B. B., Shu, S., Kumar, N. N., Weaver, J. L., Sen, J., Perez-Reyes, E., Stornetta, R. L., Guyenet, P. G., & Bayliss, D. A. (2016). Nalcn is a "Leak" sodium channel that regulates excitability of brainstem chemosensory neurons and breathing. *Journal of Neuroscience*, **36**, 8174–8187.

Shi, Y., Stornetta, D. S., Reklow, R. J., Sahu, A., Wabara, Y., Nguyen, A., Li, K., Zhang, Y., Perez-Reyes, E., Ross, R. A., Lowell, B. B., Stornetta, R. L., Funk, G. D., Guyenet, P. G., & Bayliss, D. A. (2021). A brainstem peptide system activated at birth protects postnatal breathing. *Nature*, **589**, 426–430.

Shi, Y., Stornetta, R. L., Stornetta, D. S., Onengut-Gumuscu, S., Farber, E. A., Turner, S. D., Guyenet, P. G., & Bayliss, D. A. (2017). Neuromedin B expression defines the mouse retrotrapezoid nucleus. *Journal of Neuroscience*, **37**, 11744–11757.

Souza, G., Kanbar, R., Stornetta, D. S., Abbott, S. B. G., Stornetta, R. L., & Guyenet, P. G. (2018). Breathing regulation and blood gas homeostasis after near complete lesions of the retrotrapezoid nucleus in adult rats. *Journal of Physiology*, **596**, 2521–2545.

Stornetta, R. L., McQuiston, T. J., & Guyenet, P. G. (2004). GABAergic and glycinergic presympathetic neurons of rat medulla oblongata identified by retrograde transport of pseudorabies virus and in situ hybridization. *Journal of Comparative Neurology*, **479**, 257–270.

Stornetta, R. L., Moreira, T. S., Takakura, A. C., Kang, B. J., Chang, D. A., West, G. H., Brunet, J. F., Mulkey, D. K., Bayliss, D. A., & Guyenet, P. G. (2006). Expression of Phox2b by brainstem neurons involved in chemosensory integration in the adult rat. *Journal of Neuroscience*, **26**, 10305-10314.

Teran, F. A., Massey, C. A., & Richerson, G. B. (2014). Serotonin neurons and central respiratory chemoreception: where are we now?*Progress in Brain Research*, **209**, 207–233.

Turovsky, E., Theparambil, S. M., Kasymov, V., Deitmer, J. W., Del Arroyo, A. G., Ackland, G. L., Corneveaux, J. J., Allen, A. N., Huentelman, M. J., Kasparov, S., Marina, N., & Gourine, A. V. (2016). Mechanisms of CO_2/H+ sensitivity of astrocytes. *Journal of Neuroscience*, **36**, 10750–10758.

Wang, S., Benamer, N., Zanella, S., Kumar, N. N., Shi, Y., Bevengut, M., Penton, D., Guyenet, P. G., Lesage, F., Gestreau, C., Barhanin, J., & Bayliss, D. A. (2013a). TASK-2 channels contribute to pH sensitivity of retrotrapezoid nucleus chemoreceptor neurons. *Journal of Neuroscience*, **33**, 16033–16044.

Wang, S., Shi, Y., Shu, S., Guyenet, P. G., & Bayliss, D. A. (2013b). Phox2b-expressing retrotrapezoid neurons are intrinsically responsive to H+ and CO_2. *Journal of Neuroscience*, **33**, 7756–7761.

Wu, Y., Proch, K. L., Teran, F. A., Lechtenberg, R. J., Kothari, H., & Richerson, G. B. (2019). Chemosensitivity of Phox2b-expressing retrotrapezoid neurons is mediated in part by input from 5-HT neurons. *Journal of Physiology*, **597**, 2741–2766.

Additional information

Data availability statement

The datasets generated during the current study are available from the corresponding author on reasonable request.

Competing interests

None.

Author contributions

Y.S., R.L.S., A.C.T., D.K.M., T.S.M. and D.A.B. designed research; Y.S., C.R.S., B.M.M., J.S.-P., D.S.S. and T.S.M. performed research; Y.S., C.R.S., B.M.M., J.S.-P., R.L.S., A.C.T., D.K.M., T.S.M. and D.A.B. analysed data; and all authors edited the manuscript. All authors have read and approved the final version of this manuscript and agree to be accountable for all aspects of the work in ensuring that questions related to the accuracy or integrity of any part of the work are appropriately investigated and resolved. All persons designated as authors qualify for authorship, and all those who qualify for authorship are listed.

Funding

This study was funded by the National Institutes of Health (HL074011 to R.L.S.; HL137094 to D.K.M.; HL108609 to D.A.B.). This work was supported by the São Paulo Research

Foundation (FAPESP; grants: 2019/01236-4 to A.C.T.; 2015/23376-1 to T.S.M.), the Conselho Nacional de Desenvolvimento Científico e Tecnológico (CNPq grant: 408647/2018-3 to A.C.T.) and partly financed by the Coordenação de Aperfeiçoamento de Pessoal de Nível Superior – Brasil (CAPES) – Finnancial Code 001.

Keywords

breathing, chemosensor, CO_2, *Htr7*, raphe nucleus, retrotrapezoid, serotonin

Supporting information

Additional supporting information can be found online in the Supporting Information section at the end of the HTML view of the article. Supporting information files available:

Statistical Summary Document
Peer Review History
Data set for Fig. 1*B*